miR-252 targeting temperature receptor *CcTRPM* to mediate the transition from summer-form to winter-form of *Cacopsylla chinensis*

Songdou Zhang, Jianying Li, Dongyue Zhang, Zhixian Zhang, Shili Meng, Zhen Li, Xiaoxia Liu*
Department of Entomology and MOA Key Lab of Pest Monitoring and Green Management, College of Plant Protection, China Agricultural University, 100193 Beijing, China
* Corresponding author. E-mail address: liuxiaoxia611@cau.edu.cn (Xiaoxia Liu).

Abstract:
Temperature determines the geographical distribution of organisms and affects the outbreak and damage of pests. Insects seasonal polyphenism is a successful strategy adopted by some species to adapt the changeable external environment. *Cacopsylla chinensis* (Yang & Li) showed two seasonal morphotypes, summer-form and winter-form, with significant differences in morphological characteristics. Low temperature is the key environmental factor to induce its transition from summer-form to winter-form. However, the detailed molecular mechanism remains unknown. Here, we firstly confirmed that low temperature of 10°C induced the transition from summer-form to winter-form by affecting the cuticle thickness and chitin content. Subsequently, we demonstrated that *CcTRPM* functions as a temperature receptor to regulate this transition. In addition, miR-252 was identified to mediate the expression of *CcTRPM* to involve in this behavioral transition. Finally, we found *CcTre1* and *CcCHS1*, two rate-limiting enzymes of insect chitin biosyntheis, act as the critical down-stream signal of *CcTRPM* in mediating this behavioral transition. Taken together, our results revealed that a novel signal transduction cascade mediates the seasonal polyphenism in *C. chinensis*. These findings not only lay a solid foundation for fully clarifying the ecological adaptation mechanism of *C. chinensis* outbreak, but also broaden our understanding about insect polymorphism.

Keywords: *Cacopsylla chinensis*, miR-252, *CcTRPM*, polyphenism, low temperature

Introduction

Currently, global climate change is the most important environmental problem facing with mankind, and also one of the most complex challenges in the 21st century. Insects, as the largest animal population on the earth, adapt to the complex and changeable external environment by displaying polyphenism, thus achieving the purpose of survival and reproduction (Simpson et al., 2011). Insect polyphenism is the phenomenon allows them within a given genotype to produce two or more distinct phenotypes under the challenges posed by environmental variability via beneficial shifts in morphology, behavior, or physiology (Cridge et al., 2015). Polyphenism is commonly observed in many insect species, for examples: the solitary and gregarious phases of *Locusta migratoria* (Ma et al., 2011), the short-winged and long-winged morph of *Nilaparvata lugens* (Xu et al., 2015), the wingless and winged aphid of *Acyrthosiphon pisum* (Vellichirammal et al., 2017), and the catkin and twig morphs in caterpillars of the moth *Nemoria arizonaria* (Simpson et al., 2011). With the global climate problems are increasingly prominent, the study of insect polyphenism has become a new hotspot in insect ecology, epigenetics and developmental biology.

Pear psylla is a serious pest of pear trees worldwide, including *Cacopsylla chinensis* (Yang & Li), *Psylla Betulaefoliae*, *Psylla Pyri*, and so on (Butt and Stuart, 1986; Wei et al., 2020). *C. chinensis*, belongs to Hemiptera: Psyllidae, which exclusively feeds on pear trees, harms the young shoots and leaves with adult and nymph, and secretes a large amount of honey dew to breed coal pollution bacteria of *Gloeodes pomigena* (Wei et al., 2020). It is also an important vector of the destructive disease of pear trees, *Erwinia amovora*, and currently one of the key pests in the major pear production areas in many East Asian countries, including China and Japan (Hildebrand et al., 2010; Ge et al., 2019). In most pear production areas of China, the summer-form of *C. chinensis* are usually present from April to September, whereas winter-form of *C. chinensis* are present during the rest of the year (Ge et al., 2019; Wei et al., 2020). The summer-form has lighter body color and stronger activity ability, and causes more serious damage compare with winter-form. For better adapt to the harsh environmental conditions, the eggs of summer-form develop to the winter-form before the pear fallen leaves. The winter-form has brown to dark brown body color and larger body size, but has the weaker activity ability and stronger resistance ability compare with summer-form. With the gradual increase of temperature in early spring, the winter-form lays eggs at the tender buds of pear trees and then develop into summer-form (Ge et al., 2019; Tougeron et al., 2021). Hence, the transition between summer-form and winter-form is a significant ecological strategy for *C. chinensis* to avoid adverse environmental conditions and then burst into disaster, which has prominence biological and ecological significance. The seasonal polyphenism of summer-form and winter-form in *C. chinensis* has been recognized for many years and could be induced by low temperature and short day (Oldfield, 1970; Tougeron et al., 2021), but until recently no molecular mechanism had been advanced.

Temperature is a significant factor limiting the geographic ranges of species, which determines the distribution and diffusion area of species. As a type of small poikilothermic animal, insect is sensitive to temperature changes and temperature stress response is one of the most conservative mechanism to resist extreme environment (Teets et al., 2023). Different environmental conditions affect the polyphenism of many kinds of insects, for examples, wing dimorphism of Hemiptera *Schizaphis graminum* (An et al., 2012), diapause of Lepidoptera

Bombyx mori (Tsuchiya et al., 2021) and Coleoptera *Colaphellus bowringi* (Guo et al., 2021). Under the low temperature conditions, insects can improve cold tolerance by regulating their internal energy metabolism and external exoskeleton system. Such as: darken their cuticles with melanin (Fedorka et al., 2013), thickened wax layer or chorion (Kreß et al., 2016), and store more lipids to increase energy supply and increase the accumulation of antifreeze protective substances (Terblanche et al., 2011). However, studies about how insect temperature receptor response to temperature change and then activates the downstream signal molecules to regulate the polyphenism have been very limited.

Transient receptor potential (TRP) channel family gene was firstly found in *Drosophila melanogaster* (Minke et al., 1975). The TRP channel genes involved in temperature sensing are called "thermo-sensitive TRP" or "temperature receptor" (Lee et al., 2005). In mammals, there are six thermo-sensitive TRP receptor genes, of which TRPV1-4 mainly feel moderate high temperature (Venkatachalam and Montell, 2007) and TRPM8 can be activated by low temperature (8°C-28°C) or cooling substances, such as menthol and borneol (Peier et al., 2002). The activation mode is mainly due to the depolarization of cell membrane caused by the influx of Ca^{2+} (McKemy et al., 2002). Presently, researches on the function of temperature receptor gene TRP were mainly focused on some model insects, but very few on the agricultural pests. For example, *D. melanogaster TRPM* is highly expressed in dendritic sensory neurons and can sense cold stimulation (Turner et al., 2016). In *B. mori*, high temperature receptor *BmTRPA1* regulates the diapause of offspring eggs by acting on the neuroendocrine hormone signal of GABAergic-GnRH/Crz-DH (Sato et al., 2014; Tsuchiya et al., 2021). However, studies on agricultural insects, such as *Apolygus lucorum* (Fu et al., 2016), *N. lugens* (Wang et al., 2021a), *Bemisia tabaci* (Dai et al., 2018), and *Tuta absoluta* (Wang et al., 2021b), also only focused on the identification of the related temperature receptor gene TRPs and its correlation with temperature, no detailed molecular mechanism were reported. In agricultural insects, members of TRPA subfamily are mainly responsible for answering the high-temperature stimulation (Tracey et al., 2003; Neely et al., 2011), while members of TRPM subfamily are mainly involved in low-temperature stimulation as temperature receptors (Rosenzweig et al., 2008; Turner et al., 2016). Temperature significantly affected the annual generations, adult survival rate, hibernation period and egg laying period of *C. chinensis* (Butt and Stuart, 1986). Our preliminary research results found that low temperature is the key factor to induce the transition from summer-form to winter-form in *C. chinensis*. Therefore, we speculated that *TRPM*, functions as a temperature receptor gene, may participate in the transition from summer-form to winter-form in response to low temperature, but the specific molecular mechanism needs to be further explored.

MicroRNAs (miRNAs), a class of non-coding RNA molecules, were encoded by endogenous genes in a length of about 18-25 nt. They mainly regulate many life processes, including cell differentiation, organ development, cell apoptosis, biological rhythm and metamorphosis development in animals and plants at the post-transcriptional level by inhibiting the translation process of target genes or degrading the mRNA of target genes (Asgari, 2013). In recent years, more and more studies reported that miRNAs are involved in regulating the insect polymorphism, such as the caste differentiation of honeybees, the phenotypic plasticity of *L. migratoria* and the wing pleomorphism of *N. lugens* (Liu et al., 2012; Yang et al., 2014; Ye et al., 2019). In addition, miRNAs also play important roles in insect adaptation to temperature stress. For examples, miR-7 and miR-8 involved in the process of temperature adaptation of *D. melanogaster* (Kennell et al.,

114 2012). MiRNAs were also found in responding to low temperature stress in rice water weevil
115 (*Lissorhoptrus oryzophilus*) and gall midge (*Epiblema Scudderiana*) (Yang et al., 2017a; Lyons et
116 al., 2015). There were also reported that miR-204 targeted *TRPM3* to regulate mammalian eye
117 development (Shiels, 2020), and miR-135a targeted *TRPC1* to participate in podocyte injury
118 (Yang et al., 2017b). Here, we screened and validated miR-252, a miRNA whose expression was
119 down-regulated under low temperature, negatively targeted *CcTRPM* to modulate the transition
120 from summer-form to winter-form by acting on the cuticle thickness and cuticle chitin content.
121 Chitin biosynthesis signal was also proved to involve in the transition from summer-form to
122 winter-summer in response to *CcTRPM* and miR-252. Our work not only promotes the
123 comprehensive understanding of the adaptation mechanism for *C. chinensis* outbreak at the
124 physiological and ecological level as well as the insect polymorphism, but also helpful in
125 identifying potential target genes in pest control through blocking temperature adaptation of pests.

126 **Results**

127 **Low temperature induced the transition from summer-form to winter-form in *C. chinensis***

128 *C. chinensis* was displayed as seasonal polyphenism along with seasonal changes: the
129 summer-form and the winter-form. The significant differences in morphological characteristics are
130 as following: (1) Eggs are long oval shape with a thin tip and a blunt end. Eggs of summer-form
131 are milky white at the initial stage and gradually become yellow white at the later stage (Figure
132 1A). Eggs of winter-form are mostly yellowish brown or orange (Figure 1A'). (2) The nymph has
133 five instars and its body size is gradually increasing with age. The body of the newly hatched
134 nymph is oval and the compound eyes are red. The 1st instar nymph of summer-form is light
135 yellow and transparent (Figure 1B). The 3rd and 5th instar nymphs of summer-form are
136 yellow-green or blue-yellow, and the wing buds are oblong, protruding and sticking to both sides
137 of the body (Figure 1C and 1D). The 1st instar nymph of winter-form has many black stripes on
138 the chest back plate, and the end of the abdomen and back are black (Figure 1B'). The 3rd and 5th
139 instar nymphs of winter-form are overall black brown, with dark brown stripe on the left and right
140 sides of each section on the chest and back of the abdomen, and the end of the abdomen and back
141 becomes a large piece with black brown color (Figure 1C' and 1D'). (3) The antennae of adults
142 are filamentous with 10 nodes, and the front wings are translucent and oblong. The body color of
143 summer-form adult is green or yellow-green with yellow-brown stripes on the shield of the chest
144 and back plate, and no stripes on the wings (Figure 1E). The body color of winter-form adult is
145 brown or dark brown, with dark brown stripes on the whole body, and clearly brown stripes on the
146 rear edges of the front wings (Figure 1E').

147 To clarify the effect of temperatures on the transition from summer-form to winter-form, the
148 newly-hatched 1st instar summer-form nymphs were treated with four different temperatures
149 (25°C, 20°C, 15°C, and 10°C). The results indicated that all the survived treated nymphs develop
150 to the 3rd instar summer-form nymphs at 25°C, approximately 17% and 40% of survived treated
151 nymphs develop to the 3rd instar winter-form nymphs at 20°C and 15°C, but all the survived
152 treated nymphs develop to the 3rd instar winter-form nymphs at 10°C (Figure 1F). It meant that
153 low temperature (especially 10°C) was the key environment factor to induce the transition from
154 summer-form to winter-form and 10°C was selected for the following study. In addition, two
155 cooling agents, menthol and borneol, were also used to mimic the low temperature effect of 10°C.

156 We observed that about 49% and 37% of the survived treated nymphs develop to the 3rd instar
157 winter-form nymphs after menthol and borneol treatment at 25°C, respectively (Figure 1G).
158 To further explore the differences between summer-form and winter-form nymphs, cuticle
159 thicknesses and cuticle chitin content were determined. The ultrastructure results of transmission
160 electron microscopy assays showed that cuticle thicknesses of 3rd instar winter-form (about 3.86
161 μm) were obviously higher than 3rd instar summer-form (about 1.82 μm) (Figure 1H and 1I). We
162 also found that winter-form nymphs exhibited higher chitin level in cuticle compared to the
163 summer-form nymphs by using the WGA-FITC staining and chitin content determination (Figure
164 1J and 1K). Taken together, these findings demonstrated that low temperature of 10°C induced the
165 transition of summer-form to winter-form by affecting the cuticle thicknesses and cuticle chitin
166 content.
167
168 ***CcTRPM* is a conventional cold-sensing TRP channel activated by 10°C in *C. chinensis***
169 A cDNA fragment, which was putatively encoded a cold-sensing TRPM channel gene, was
170 identified as *CcTRPM* from *C. chinensis*. The full-length sequence of *CcTRPM* was amplified and
171 verified by RT-PCR with specific primers (Table S1) and sequencing. Sequence analysis
172 displayed that the ORF of *CcTRPM* was 4566 bp with a 455 bp 3'UTR and encoded a deduced
173 polypeptide of 1521 amino acids with six transmembrane domains. Multiple alignment analysis of
174 the amino acid sequence indicated that the transmembrane domains of *CcTRPM* shared very high
175 amino acid identity with TRPM sequences from other five selected insect species (Figure S1A).
176 As shown in Figure S1B, phylogenetic analysis revealed that *CcTRPM* was most closely related to
177 the *DcTRPM* homologue (*Diaphorina citri*, XP_017299512.2), which was consistent with the
178 evolutionary relationships predicted from the multiple alignment of amino acid sequences. The
179 potential tertiary protein structure of *CcTRPM* was constructed with the online server Phyre[2] and
180 modified with PyMOL-v1.3r1 software, and the conserved ankyrin repeats (ANK) and six
181 transmembrane domains were identified (Figure 2A).
182 The results of temperature treatment indicated that the mRNA expression of *CcTRPM* was
183 obviously induced by 10°C treatment at 3, 6, and 10 days compared with 25°C treatment by
184 qRT-PCR (Figure 2B). It is well known that the TRPM subfamily channels in vertebrates are
185 activated by a variety of chemical compounds, including menthol (Peier et al., 2002). We
186 therefore attempted to identify chemical compounds that either activate or inhibit *CcTRPM*.
187 qRT-PCR results revealed that menthol treatment with all three concentrations significantly
188 increased the mRNA expression of *CcTRPM* and antagonist (HY-112430, MedChemExpress,
189 Shanghai, China) treatment with all three concentrations markedly reduced *CcTRPM* transcription
190 (Figure S2F-S2G). To further confirm *CcTRPM* is a cold-sensing TRP channel gene, fluorescence
191 detection of Fluo-4 AM and Ca^{2+} imaging was performed to determine whether
192 CcTRPM-expressing cells increased intracellular Ca^{2+} concentration upon menthol treatment. The
193 results of fluorescence detection of Fluo-4 AM indicated that there was no change of Ca^{2+}
194 concentration in CcTRPM-expressing cells was treated with DMSO, but a clear increase of Ca^{2+}
195 concentration was observed when treated with menthol which was similar with the trend of
196 pcDNA-expressing cells was treated with the positive control of ionomycin (Figure 2C). The
197 effect of menthol on *CcTRPM* was further tested using Ca^{2+} imaging and showed that menthol
198 obviously elevated intracellular Ca^{2+} levels in CcTRPM-expressing cells (Figure 2D). We
199 therefore concluded that *CcTRPM* is a cold-sensitive ion channel activated by 10°C low

200 temperature and menthol.
201
202 ***CcTRPM* modulated the transition from summer-form to winter-form of *C. chinensis* in**
203 **response to low temperature**
204 Temporal expression profiles by qRT-PCR revealed that *CcTRPM* mRNA expressed in all
205 determined stages, with the highest expression level in the 1st instar nymph, and showed a
206 decreased trend from 2nd instar nymph to adult 1 day (Figure 2E). The FISH results also indicated
207 that *CcTRPM* mRNA has a greatest expression level in the 1st instar nymph and relative lower
208 expression in the 3rd and 5th instar nymph (Figure 2F).
209 To study whether *CcTRPM* modulated the transition from summer-form to winter-form of *C.*
210 *chinensis*, the newly-hatched 1st instar nymphs of summer-form were fed with dsCcTRPM or
211 dsEGFP. For the RNAi efficiency under 10°C condition, feeding of dsCcTRPM reduced the
212 transcription level of *CcTRPM* by about 61% and 62% compare to dsEGFP feeding at 3 d and 6 d
213 by qRT-PCR (Figure S3A), and decreased the CcTRPM-Cy3 signal at 6 d by FISH (Figure S3B).
214 Both results of cuticle ultrastructure and cuticle chitin content determination showed that cuticle
215 thicknesses (about 1.97 μm) and cuticle chitin content of dsCcTRPM-treated nymphs were
216 markedly lower than dsEGFP-treated nymphs (about 3.71 μm) under 10°C condition (Figure 2G
217 and 2H). Additionally, dsCcTRPM feeding and *CcTRPM* antagonist treatment both significantly
218 decreased the transition percent from summer-form to winter-form, but menthol feeding only
219 partially rescued the transition percent and morphological phenotype under dsCcTRPM feeding
220 (Figure 2I and 2J). To exclude the effect of *CcTRPM* itself on the transition percent and nymph
221 development, we also performed the RNAi assays under 25°C condition. After successfully
222 interfered the mRNA expression of *CcTRPM*, the nymph development and morphological
223 phenotype were not affected compared to the dsEGFP treatment (Figure S3C-S3D). Together,
224 these findings indicated that *CcTRPM* functions as a molecular switch to modulate the transition
225 from summer-form to winter-form of *C. chinensis* in response to low temperature.
226
227 **Confirming of miR-252 targeted *CcTRPM***
228 To explore the regulation mechanism of *CcTRPM* at the post-transcriptional level, two
229 software programs of miRanda and Targetscan were used to predict the potential miRNAs. There
230 are four miRNAs (miR-252, miR-5728, PC-3p-173924, and PC-3p-137568) were predicted to
231 have the corresponding target-binding sites with the 3'UTR of *CcTRPM* (Figure 3A and S4A).
232 miR-252 showed the opposite expression patterns with *CcTRPM* after 25°C and 10°C treatments
233 (Figure 2B and 3B). To further determine whether miR-252 specifically targeted *CcTRPM*, the
234 following four experimental approaches were performed: (1) The dual-luciferase reporter assays
235 were carried out by cloning a 419 bp 3'UTR fragment of *CcTRPM* containing the predicted target
236 binding sites of the miRNAs. The relative luciferase activities were obviously decreased when the
237 agomir-252 and CcTRPM-3'UTR-pmirGLO were cotransfected, while the activity recovered to
238 the control when using the mutated 3'UTR sequence without the binding sites of miR-252 (Figure
239 3C). However, the relative luciferase activities were no change when the construct of
240 CcTRPM-3'UTR-pmirGLO was cotransfected with the agomir of other three miRNAs,
241 respectively (Figure S4B). (2) An RNA immunoprecipitation assay indicated that the transcripts of
242 *CcTRPM* and miR-252 increased 6.35-fold and 9.21-fold from the agomir-252 feeding nymphs of
243 the Ago-1 antibody-mediated RNA complex compared to an IgG control, separately (Figure 3D

244 and S5). (3) FISH results showed that *CcTRPM* and miR-252 were co-expressed in the nymphs
245 and displayed an opposite expression trend along with the increasing instar (Figure 3E). (4)
246 qRT-PCR results indicated that agomir-252 feeding significantly inhibited *CcTRPM* mRNA
247 expression and antagomir-252 feeding markedly increased *CcTRPM* mRNA expression compare
248 to their controls, separately (Figure 3F). These data together confirmed that miR-252 directly
249 targeted *CcTRPM*.
250
251 **miR-252 mediated the transition from summer-form to winter-form in *C. chinensis* by**
252 **suppressing *CcTRPM***
253 To test the efficiency of agomir-252, 1st instar nymphs of summer-form were fed with
254 agomir-252 under 10°C condition. qRT-PCR results showed that miR-252 expression was both
255 significantly increased after agomir-252 treatment at 3 d and 6 d (Figure 4A). To further clarify
256 the relationship between *CcTRPM* and miR-252, we determined miR-252 expression after
257 dsCcTRPM treatment under 10°C condition. Interestingly, miR-252 expression was dramatically
258 inhibited after successful interference of *CcTRPM* at 3 d and 6 d (Figure 4B). This result implied
259 that up-regulation of *CcTRPM* expression may have a positive feedback to miR-252 expression in
260 response to 10°C temperature.
261 To deeply decipher the role of miR-252 in the transition from summer-form to winter-form,
262 1st instar nymphs of summer-form were fed with agomir-NC or agomir-252 under 10°C condition.
263 Results of cuticle ultrastructure indicated that cuticle thickness of agomir-252 treated nymphs
264 (about 1.85 μm) was markedly lower than agomir-NC treated nymphs (about 3.70 μm) (Figure 4C
265 and 4D). Both WAG-FITC staining and chitin content determination revealed that cuticle chitin
266 content of agomir-252 treated nymphs were obviously lower than agomir-NC treated nymphs
267 (Figure 4E and 4F). Moreover, agomir-252 feeding significantly decreased the transition percent
268 from summer-form to winter-form, but antagomir-252 feeding rescued the defect of transition
269 percent and morphological phenotype under dsCcTRPM treatment (Figure 4G and 4H). To further
270 evaluate the effect of agomir-252 under 25°C condition, we determined *CcTRPM* expression and
271 observed the nymph development after agomir-252 feeding. As expected, *CcTRPM* expression
272 was still significantly decreased after agomir-252 feeding (Figure S6C), but the nymph
273 development and morphological phenotype were not affected by agomir-252 treatment compared
274 to the agomir-NC treatment (Figure S6D). Above all, these results displayed that miR-252
275 mediated the transition from summer-form to winter-form in *C. chinensis* by suppressing
276 *CcTRPM* via affecting the cuticle thickness and cuticle chitin content.
277
278 **Chitin biosynthesis signaling involved in the transition from summer-form to**
279 **winter-summer of *C. chinensis* in response to low temperature and *CcTRPM***
280 Since cuticle thickness and cuticle chitin content were obviously affected by dsCcTRPM
281 treatment and agomir-252 treatment, we speculated that chitin biosyntheis signaling pathway
282 participated in the transition from summer-form to winter-form. To demonstrate this hypothesis, a
283 total of 14 transcripts corresponding to 8 genes involved in chitin biosyntheis were identified in *C.*
284 *chinensis*, with several genes were present in two or more paralogous forms (Figure 5A). Next, we
285 used qRT-PCR to determine the expression profiles of these 14 chitin biosyntheis transcripts after
286 25°C and 10°C treatments at 3 d, 6 d, and 10 d. Based on the relative gene expression in the heat
287 map, we found that the expression of 13 transcripts exhibited overall up-regulation under 10°C

288 condition at 3 d, 6 d, and 10 d compared to those under 25°C condition, while levels for CcUAP2
289 were almost unchanged (Figure 5B).
290 Subsequently, we used RNAi to further uncover the impact of chitin biosyntheis genes in the
291 transition from summer-form to winter-form. Compared with dsEGFP feeding control, only
292 knockdown of *CcTre1* and *CcCHS1* obviously decreased the transition percent from summer-form
293 to winter-form, but not by knockdown of the remaining transcripts (Figure 5C). To further dissect
294 the roles of *CcTre1* and *CcCHS1*, cuticle thickness and cuticle chitin content were also determined.
295 Compared with dsEGFP feeding control, knockdown of *CcTre1* and *CcCHS1* markedly reduced
296 the cuticle thickness and cuticle chitin content (Figure S7C-S7D, 5D-5F), which were similar with
297 dsCcTRPM feeding and agomir-252 treatment. To confirm whether *CcTre1* and *CcCHS1* function
298 as the downstream of *CcTRPM* and miR-252, we next determine the expression of *CcTre1* and
299 *CcCHS1* after *CcTRPM* knockdown and agomir-252 feeding. qRT-PCR results indicated that
300 *CcTRPM* knockdown and agomir-252 feeding were both obviously reduced the mRNA expression
301 of *CcTre1* and *CcCHS1* at 3 d and 6 d, respectively (Figure 5G-5J). These phenotypic and
302 molecular data suggested that chitin biosynthesis signaling involved in the transition from
303 summer-form to winter-summer of *C. chinensis* in response to low temperature and *CcTRPM*.

304 **Discussion**

305 Polyphenism offers the opportunity for insects to deploy different phenotypes generated from
306 the same genome to best suit the extreme environmental changes (Simpson et al., 2011). In recent
307 years, studies on insect polyphenism have mainly focused on the molecular regulation by
308 endocrine hormones, neuropeptides, and neurotransmitters, while the regulation mechanism by
309 external environmental factors remains poorly understood. For examples, ecdysone signaling and
310 insulin/IGF signaling pathway regulated the wing polyphenism of pea aphid (Vellichirammal et al.,
311 2017) or planthoppers (Zhang et al., 2022), neuropeptide F was essential for shaping locomotor
312 plasticity in locust (Hou et al., 2017), and dopamine metabolic pathway modulated the behavioral
313 phase changes of the migratory locust (Ma et al., 2011). Temperature is important in defining the
314 distribution of insects, but how it activates the temperature receptor and then regulates
315 polyphenism need further deeply study. Here, we firstly demonstrated that the transition from
316 summer-form to winter-form in *C. chinensis* was "temperature-dependent pattern", and low
317 temperature of 10°C completely induced this transition. Just like people wear more clothes in the
318 winter, we also proved that 10°C induced the summer-form change to winter-form by increasing
319 the cuticle thickness and cuticle chitin content. Several similar phenotype changes have been
320 reported in other insects: the cricket of *Allonemobius socius* exhibited darker cuticles to improve
321 thermo-regulation in colder environments (Fedorka et al., 2013), the mosquito of *Aedes albopictus*
322 increased the thickness of the egg middle serosa cuticle and wax layer as an adaptation strategy for
323 cold acclimation (Kreß et al., 2016).
324 TRPM8, a member of the TRP family, has been reported as the principal sensor of
325 environmental cold in mammals (Peier et al., 2002). As a kind of poikilothermic animals, insects
326 also have an evolutionarily conserved TRPM gene which is homologous to mammalian
327 temperature receptor of TRPM8 (Venkatachalam and Montell, 2007). In this study, we identified a
328 classical TRPM gene in *C. chinensis* which was designated as *CcTRPM* and functioned as a low
329 temperature receptor by using qRT-PCR and calcium imaging. After knockdown of *CcTRPM* by

330 feeding dsCcTRPM, the treated nymphs displayed thinner cuticle thickness and less cuticle chitin
331 content compared with the control of dsEGFP treatment under 10°C condition. In addition,
332 *CcTRPM* knockdown by RNAi or *CcTRPM* antagonist feeding both caused obvious defect of the
333 transition percent from summer-form to winter-form, but this defect could be partially rescued by
334 a cooling agent menthol treatment. To exclude the developmental defect or genetic background,
335 we also knocked down *CcTRPM* under 25°C condition, and not found any death defect and cuticle
336 defect. These results were the first report about *CcTRPM* was essential for insect polyphenism in
337 response to low temperature. Until now, the researches about TRPM on other agricultural insects
338 only focused on the description of its correlation with temperature, but no deeply molecular
339 function was reported (Fu et al., 2016; Wang et al., 2021a). Therefore, the molecular regulation
340 mechanism of *CcTRPM* in response to low temperature needs further study.
341 miRNAs played significant roles in insect polyphenism and cold acclimation. For example,
342 miR-34 and miR-9b mediated the wing dimorphism of *N. lugens* (Ye et al., 2019) and *A. citricidus*
343 (Shang et al., 2020), miR-133 inhibited behavioral aggregation by controlling dopamine synthesis
344 in *L. migratoria* (Yang et al., 2014), and miR-31-5p via asc-C9 to regulate cold acclimation in
345 *Monochamus alternatus* (Zhang et al., 2020). Here, we demonstrated that a key regulator,
346 miR-252, targets *CcTRPM* via a negative feedback loop to control the transition from
347 summer-form to winter-form in response to low temperature. Interestingly, RNAi-mediated
348 knockdown of *CcTRPM* also decreased the expression of miR-252. This result implied that
349 up-regulation of *CcTRPM* in response to low temperature may be have a feedback to miR-252,
350 then miR-252 inhibits the expression of *CcTRPM* under low temperature condition to avoid its
351 excessive expression. Upon miR-252 agomir feeding, the treated nymphs showed thinner cuticle
352 thickness and less cuticle chitin content compared with the control of agomir-NC feeding under
353 10°C condition. Besides, miR-252 antagomir feeding could rescue the transition percent defect
354 and morphological phenotype defect caused by *CcTRPM* knockdown. These results were the first
355 report about miR-252 functions as the up-stream regulator to control the transition from
356 summer-form to winter-form in response to low temperature via acting on the insect cuticle
357 thickness and cuticle chitin content. Similar result was reported in *Daphnia pulex*, miR-252 might
358 increase cadmium tolerance by switching cellular growth and cuticle protein pathways to
359 detoxification processes (Chen et al., 2016). In *Leptinotarsa decemlineata*, 42 differentially
360 expressed miRNAs were identified following cold exposure including miR-9a-3p, miR-210-3p,
361 miR-276-5p and miR-277-3p (Morin et al., 2017). Therefore, the regulatory network of miRNAs
362 is need further investigating in the transition between two phases in *C. chinensis*, especially
363 transboundary miRNAs from host plant.
364 Insect cuticle serves as a protective barrier and plays significant roles in supporting the body,
365 resisting the adverse environmental conditions, preventing predators from predation, and
366 preventing pathogens from invading (Evans and Sanson, 2005; Vargas et al., 2014). Chitin as an
367 extremely important structural component of insects and represents up to 60% of the dry weight in
368 some species (Richards, 1978). Many studies have reported that insect cuticles are essential for
369 cold acclimation (Fedorka et al., 2013; Kreß et al., 2016). In this study, cuticle thickness and
370 cuticle chitin content were the major differences between summer-form and winter-form. We have
371 demonstrated that *CcTRPM* and miR-252 function as the up-stream signaling to mediate the
372 transition from summer-form to winter-form in response to low temperature via affecting the
373 cuticle thickness and cuticle chitin content. Therefore, it is necessary to study whether chitin

374 biosynthesis pathway acting as the down-stream signaling in this transition. Further RNAi results
375 showed that two rate-limiting enzyme genes, *CcTre1* and *CcCHS1*, play essential roles in the
376 transition from summer-form to winter-form in response to low temperature and affect the cuticle
377 thickness and cuticle chitin content. In addition, *CcTRPM* knockdown and miR-252 agomir
378 feeding both markedly decreased the mRNA expression of *CcTre1* and *CcCHS1*. These results
379 proved our hypothesis and were the first report that chitin biosynthesis pathway functions as the
380 down-stream signaling to control the transition from summer-form to winter-form in *C. chinensis*.
381 In summary, this study reported a novel signaling pathway of low
382 temperature-miR-252-*CcTRPM* acting on cuticle chitin biosynthesis genes to mediate the
383 transition from summer-form to winter-form in *C. chinensis*. We proposed a working model to
384 describe this novel mechanism in Figure 6. Under 25°C condition, the expression of temperature
385 receptor *CcTRPM* was depressed by miR-252, so the 1st instar nymphs of summer-form normally
386 developed into 3rd instar nymphs of summer-form. However, under 10°C condition, low
387 temperature greatly activated the expression of *CcTRPM*, but miR-252 functioned as a negative
388 feedback regulator to mediate *CcTRPM* expression to avoid its excessive expression in response to
389 low temperature. Then, *CcTRPM* obviously improved the expression of two rate-limiting enzyme
390 genes from cuticle chitin biosynthesis pathway, *CcTre1* and *CcCHS1*, to increase cuticle thickness
391 and raise cuticle chitin content. Lastly, the 1st instar nymphs of summer-form developed to 3rd
392 instar nymphs of winter-form as an ecological adaptation strategy under low temperature stress.
393 Future researches will focus on the following directions: (1) Whether and how transboundary
394 miRNAs and hormones from host plant involve in the transition from summer-form to
395 winter-form in *C. chinensis*. (2) How neuropeptides and endocrine hormones response to low
396 temperature and *CcTRPM* to mediate the transition from summer-form to winter-form in *C.*
397 *chinensis*.

398 **Materials and Methods**

399 **Insects and host plants**

400 The summer-form and winter-form colonies of *C. chinensis* (Yang & Li) were initiated
401 collected in June and December 2018 from a pear orchard in Daxing district, Beijing, China,
402 respectively. These two populations are now reared in the integrated pest management (IPM)
403 laboratory of China Agricultural University. The summer-form population was raised in growth
404 chambers at 25 ± 1°C under a photoperiod of 12L: 12D with 65 ± 5% RH (relative humidity). The
405 feeding conditions of winter-form population were raised at 10 ± 1 ° C under a photoperiod of 12L:
406 12D with 25 ± 5% RH. Unless otherwise specified, the photoperiod of all the following different
407 temperature treatments is 12L: 12D.
408 Host plants were 2-3 years old Korla fragrant pear seedlings with a height of 60-100 cm
409 under conventional water and fertilizer management.
410

411 **Different temperatures and cooling agents induced the transition from summer-form to**
412 **winter-form**

413 For different temperatures treatment, the newly-hatched 1st instar summer-form nymphs
414 (within 12 h) were transferred to the young vegetative shoots of healthy Korla fragrant pear
415 seedlings at four different temperatures (25°C, 20°C, 15°C, and 10°C) by using a fine brush. Then,

416 observed the morphological characteristics every two days, and counted the number of
417 summer-form and winter-form individuals according to the body color and external characteristics
418 until the 3rd instar. Each treatment was performed with three independent biological replications
419 of at least 30 nymphs for each biological replication.
420 Menthol (HY-N1369) was purchased from MedChemExpress LLC (Shanghai, China) and
421 borneol (420247) was bought from Sigma-Aldrich LLC (Saint Louis, USA) (Figure S2A-S2B)
422 (Peier et al., 2002; Turner et al., 2016). For the treatment of different cooling agents, feeding setup
423 through a pear leaf was used as previously described in *Aphis citricidus* with minor adjustment
424 (Shang et al., 2020). Briefly, a stem with a fresh pear leaf was inserted into a sterile PCR tube of
425 250 μL containing 200 μL of menthol (1 mg/mL) or borneol (0.1 mg/mL). Then, the PCR tube
426 with leaf was transferred to a 50 mL sterile plastic tube, termed as stem-leaf device. Finally,
427 transferred the newly-hatched 1st instar summer-form nymphs (within 12 h) into the stem-leaf
428 device, observed the morphological characteristics every two days, and counted the number of
429 summer-form and winter-form individuals according to the body color and external characteristics
430 until the 3rd instar under 25°C. Each treatment was performed with three independent biological
431 replications of at least 30 nymphs for each biological replication.
432
433 **Transmission electron microscopy assay of cuticle**
434 To analyze the difference of nymph cuticle ultrastructure and thickness between different
435 samples, transmission electron microscopy was used as previously described (Ekino et al., 2017;
436 Ge et al., 2019). Briefly, samples were firstly fixed in 4% polyformaldehyde (PFA) for 48 h and
437 followed by post-fixation in 1% osmium tetroxide for 1.5 h. Next, the samples were dehydrated in
438 a standard ethanol/acetone series, infiltrated and embedded in spurr resin embedding medium.
439 Then, the superthin sections (-70 nm) were cut and stained with 5% uranyl acetate followed by
440 Reynolds' lead citrate solution. Finally, the sections were observed, photographed and measured
441 under a Hitachi HT7800 transmission electron microscope operated at 120 kv. Five nymphs were
442 used for each sample.
443
444 **Cuticle chitin staining assay with WGA-FITC and determination of cuticle chitin content**
445 Previous studies have demonstrated that cuticle thickness and hardness are important
446 parameters for adapting to environment and natural enemies (Evans and Sanson, 2005). Therefore,
447 cuticle chitin staining with WGA-FITC (Cat# F8520, Solarbio, Beijing, China) and cuticle chitin
448 content were measured to analyze the difference between the summer-form and winter-form
449 nymphs, or dsRNA treatment and miRNA agomir treatment. For the WGA-FITC staining, nymph
450 samples were firstly fixed with 4% PFA for 48 h and dehydrated with a series of sucrose solution
451 with varied concentrations (10% for 4 h, 20% for 4 h, 30% for 12 h), then rinsed three times for 15
452 min per rinse with sterile PBS buffer. The dehydrated samples were gradually embedded in
453 Tissue-Tek O.C.T. compound (Cat# 4583, SAKURA, Ningbo, China) after the pre-embedding
454 stages under -25°C. The ultra-thin sections (approximately 70 nm thickness) of embedded material
455 were cut using Leica freezing ultra-cut microtome (CM1850, Leica, Weztlar, Germany). The
456 sections were stained with WGA-FITC (50 μg/mL) and DAPI (10 μg/mL) for 15 min and then
457 rinsed three times for 15 min per rinse with sterile PBS buffer as previously described (Farnesi et
458 al., 2012; Xie et al., 2022). Fluorescence images were acquired using a Leica SP8 confocal
459 microscopy (Weztlar, Germany).

460 For the determination of cuticle chitin content, chitin Elisa kit (Cat# YS80663B, Yaji
461 Biotechnology, Shanghai, China) was used according to the manufacturer's instruction. In short,
462 each 50 nymphs for one sample were homogenized in 0.2 mL distilled water using an electric
463 homogenizer. The testing samples and standard samples were hatched in enzyme-labeled plates at
464 37°C for 30 min, separately. The washing buffer was used to rinse the enzyme-labeled plates five
465 times for 30 s per time. Then, enzyme labeling reagent was added to the plates for hatching and
466 washing. Finally, chromogenic agent A solution and B solution were mixed in holes for coloration
467 at 37°C and protect from light. The absorbance (OD value) of each hole was measured at 450nm
468 wavelength and zeroed with a blank hole.
469
470 **Sequence characterization of *CcTRPM***
471 The GenBank accession number of *CcTRPM* was OQ658558. The tertiary protein structures
472 of *CcTRPM* was predicted with online server Phyre[2]
473 (http://www.sbg.bio.ic.ac.uk/phyre2/html/page.cgi?id=index) and modified with PyMOL-v1.3r1
474 software. NCBI database was used to search the homologous protein sequences of *CcTRPM* from
475 various species. Multiple alignments of the amino acid sequences for *CcTRPM* with other
476 homologies was performed using DNAman software. Phylogenetic analysis was carried out based
477 on the neighbor-joining (NJ) method using MEGA10.1.8 software.
478
479 **qRT-PCR for mRNAs and miRNAs**
480 To examine the temporal expression profile of *CcTRPM*, summer-form samples were
481 collected at different developmental stages, including egg; nymphs of the 1st, 2nd, 3rd, 4th, and
482 5th instar; adults of 1, 5, and 10 days. For the effect of different temperatures treatment on the
483 mRNA expression of *CcTRPM*, miR-252, and chitin biosynthesis signaling genes, summer-form
484 1st instar nymphs were treated at 25°C and 10°C. Samples of nymphs were collected at 3, 6, and
485 10 days after different temperatures treatment and immediately stored at -80°C. Each sample was
486 performed in three replications, with about 100 individuals for each replication of egg samples and
487 at least 50 insects were included for each nymph or adult samples. All samples were immediately
488 stored at -80°C for total RNA extraction.
489 Total RNA was isolated from the above samples using TRNzol Universal (Cat# DP424,
490 TIANGEN, Beijing, China) and miRcute miRNA isolation kit (Cat# DP501, TIANGEN, Beijing,
491 China) for mRNA and miRNA according to the manufacturer' instruction, respectively. The
492 first-strand cDNAs of mRNA and mature miRNA were synthesized from 500 ng of total RNA
493 using PrimeScript™ RT reagent kit with gDNA Eraser (Cat# RR047A, Takara, Kyoto, Japan) and
494 miRcute Plus miRNA First-Strand cDNA Synthesis Kit (Cat# KR211, TIANGEN, Beijing, China)
495 following the instruction manual. The relative expression of mRNA and miRNA was respectively
496 quantified using TB Green® *Premix Ex Taq*™ II (Tli RNaseH Plus) (Cat# RR820A, Takara, Kyoto,
497 Japan) and miRcute Plus miRNA qPCR Detection Kit (Cat# FP411, TIANGEN, Beijing, China)
498 in a 20 μL reaction mixture on a Bio-Rad CFX Connect™ Real-Time PCR System (Bio-Rad,
499 Hercules, CA, USA). To reduce the error, two reference genes of *C. chinensis*, *Ccβ-actin*
500 (GenBank accession number: OQ658571) and *CcEF-1* (GenBank accession number: OQ658572),
501 were used as internal controls for real-time PCR. U6 snRNA of *C. chinensis* was used as reference
502 gene for miRNA expression. To check for the specificity, melting curves were analyzed for each
503 data point (Figure S2, S6-S7). The specific reverse primer for miRNA expression was

504 complementary to the poly (T) adapter that was provided in the miRcute plus miRNA qPCR
505 detection kit. qRT-PCR data were quantified using the $2^{-\Delta\Delta CT}$ method, where ΔΔCT is equal to
506 $\Delta CT_{treated\ sample}$ -$\Delta CT_{control}$ (Livak and Schmittgen, 2001).
507
508 **Ca^{2+} imaging and fluorescence detection of Fluo-4 AM**
509 The ORF sequence of *CcTRPM* was amplified by PCR with specific primers shown in Table
510 S1 and inserted into the pcDNA3.1(+)-mCherry vector to construct the recombinant vector of
511 CcTRPM-pcDNA3.1-mCherry using the *pEASY*®-Basic Seamless Cloning and Assembly Kit
512 (Cat# CU201, TransGen, Beijing, China). This recombinant vector was transfected into HEK293T
513 cells using TransIntro® EL Transfection Reagent (Cat# FT201, TransGen, Beijing, China) and the
514 cells were cultured for 20-40 h at 37°C. These transient-transfected cells were incubated in 500 μL
515 Fluo-4 AM (Cat# S1061, Beyotime, Shanghai, China) for 30 min at 37°C for staining and washed
516 for three times with Hank's Balanced Salt Solution. Then, these cells were treated with different
517 cooling agents and used for Ca^{2+} imaging by a Leica SP8 confocal microscopy (Weztlar, Germany)
518 or for fluorescence detection of Fluo-4 AM by a Molecular Devices i3x microplate reader (San
519 Jose, USA).
520
521 **Fluorescence *in situ* hybridization (FISH)**
522 FISH experiment was carried out as previously described with minor adjustment (Kliot et al.,
523 2014). Briefly, 20 nymphs for each sample were immersed in Carnoy's fixative (glacial acetic acid:
524 ethanol: chloroform, 1: 3: 6, vol/vol/vol) inside eppendorf tubes for at least 48 h at room
525 temperature. The fixed samples were washed with 50% ethanol for three times and decolorized in
526 6% H_2O_2 in ethanol for 48 h at room temperature. Prehybridization was performed with three
527 times for 10 min per time using the hybridization buffer (20 mM Tris-HCl, pH 8.0; 0.9 M NaCl;
528 0.01% sodium dodecyl sulfate; 30% formamide) without the probe in the dark. The probe
529 sequences of *CcTRPM*-Cy3 and miR-252-FAM are listed in Table S1 and synthesized in
530 GenePharma (Shanghai, China). Hybridize samples for 12 h in the dark in hybridization buffer
531 containing 1 μM fluorescent probe. Combine two probes with different fluorescent dyes for the
532 co-localization. After washing three times with PBST, cell nuclei were stained with DAPI (1
533 μg/mL) for 15 min and rinsed with PBST for 15 min. At last, the samples were transferred to the
534 microscope slide, mounted in mounting medium using a cover slip, and viewed under a Leica SP8
535 confocal microscopy (Weztlar, Germany). The dsCcTRPM treated samples or no-probe samples
536 were used as negative controls for the specificity of probe signal.
537
538 **dsRNA synthesis and RNAi assay**
539 Double-stranded RNAs (dsRNAs) of *EGFP*, *CcTRPM*, and 14 transcripts of chitin
540 biosynthesis signaling genes were prepared in vitro using primers ligated with T7 RNA
541 polymerase promoter sequences (Table S1) using MEGAscript™ RNAi kit (AM1626, Ambion,
542 California, USA). dsRNAs were further purified with MEGAclear columns (Ambion) and eluted
543 with diethyl pyrocarbonate (DEPC)-treated nuclease-free water. The purity and concentration of
544 dsRNA were then measured via ultraviolet spectrophotometry and gel electrophoresis. The above
545 stem-leaf device was used for dsRNA feeding and RNAi assay.
546 For the RNAi assays, summer-form 1st instar nymphs were fed with different dsRNAs (500
547 ng/μL) and divided into three groups. (1) The samples were collected after dsRNAs feeding at 2 d

548 and 4 d under 25°C condition, and at 3 d and 6 d under 10°C condition, then for the RNAi
549 efficiency analysis and miR-252 expression by qRT-PCR. (2) Observed the morphological
550 characteristics every two days and counted the number of summer-form and winter-form
551 individuals based on the above description until the 3rd instar under 10°C condition. (3) The
552 samples were collected after dsRNA feeding at 12 d for cuticle ultrastructure comparison, cuticle
553 chitin staining with WGA-FITC, and determination of cuticle chitin content under 10°C condition
554 according to the above methods.
555 For the rescue by menthol feeding under dsCcTRPM treatment, summer-form 1st instar
556 nymphs were fed with the mixture of dsCcTRPM (500 ng/μL) and menthol (1 mg/mL), then
557 counted the number of summer-form and winter-form individuals following the above method
558 until the 3rd instar under 10°C condition. All the experiments were performed in three replications
559 with at least 30 nymphs for each replication.
560
561 **Prediction of miRNAs for *CcTRPM***
562 The 3'UTR sequence of *CcTRPM* gene was amplified by the 3'-Full RACE Core Set with
563 PrimeScript™ RTase kit (Cat# 6106, Takara, Kyoto, Japan). miRNAs for *CcTRPM* were
564 predicted by a service provider LC science with two software programs of miRanda
565 (http://www.microrna.org) and Targetscan (https://www.targetscan.org/vert_72/) with the default
566 parameters (Enright et al., 2003; Agarwal et al., 2015). For software miRanda, the alignment
567 scores of 145 and -15 kcal/mol were set to the threshold. The context score percentile of
568 Targetscan was set as larger than 50 to evaluate the target relationship between miRNA and
569 potential targets. The overlapped miRNAs predicted through both methods were selected.
570
571 ***In vitro* luciferase activity assay**
572 The 419 bp sequence of 3'UTR containing predicted target sites for miR-252 in *CcTRPM*
573 was cloned into the pmirGLO vector (Promega, Wisconsin, USA) downstream of the luciferase
574 gene to construct the recombinant plasmid of CcTRPM-3'UTR-pmirGLO using the *pEASY*®-Basic
575 Seamless Cloning and Assembly Kit. The mutated 3'UTR sequence was amplified and cloned into
576 the pmirGLO vector to generate the CcTRPM-3'UTR mutant-pmirGLO plasmid. The agomir and
577 antagomir of miRNAs were chemically synthesized and modified by GenePharma (Shanghai,
578 China) with chemically modified RNA oligos of the same sequence or anti-sense oligonucleotides
579 of the miRNA. The negative control for agomir and antagomir was provided by the manufacturer.
580 HEK293T cells were cultured in a 24-well plate at 37°C in 5% CO_2 overnight and transfected with
581 CcTRPM-3'UTR-pmirGLO plasmid (approximate 500 ng) or CcTRPM-3'UTR mutant-pmirGLO
582 plasmid (approximately 500 ng) and 275 nM agomir-miRNA or agomir-NC using the Calcium
583 Phosphate Cell Transfection Kit (Cat# C0508, Beyotime, Nanjing, China). The activity of the two
584 luciferase enzymes was measured 24 h after co-transfection following the manufacturer's
585 instruction of Dual-Luciferase® Reporter Assay System (Cat# E1910, Promega, Wisconsin, USA).
586 Nine biological replications were carried out for each transfection.
587
588 ***In vivo* RNA-binding protein immunoprecipitation Assay (RIP)**
589 A Magna RIP Kit (Cat# 17-704, Merck, Millipore, Germany) was used to perform the RIP
590 assay following the manufacturer's instruction. Specifically, approximately 50 summer-form 1st
591 instar nymphs were fed with agomir-252 or agomir-NC for 24 h. The treated nymphs were

592 collected and crushed with an auto homogenizer in ice-cold RIP lysis buffer, then stored at -80°C
593 overnight. Next, 50 μL magnetic beads were incubated with 5 μg of Ago-1 antibody (Merck,
594 Millipore, Germany) or IgG antibody (Merck, Millipore, Germany) to form bead-antibody
595 complex. The frozen lysates were thawed and centrifuged, and the supernatants were divided into
596 three equal parts. One part is considered as an "input" sample and stored at -80°C for qRT-PCR
597 analysis. The other two parts were incubated with the magnetic bead-antibody complex
598 (anti-Ago1 or IgG) at 4°C overnight. The immunoprecipitated RNAs were released by digestion
599 with protease K and extracted by the above methods. Finally, the abundance of *CcTRPM* and
600 miR-252 were quantified by qRT-PCR. The "input" samples and IgG controls were assayed to
601 normalize the relative expression of target genes and ensure the specificity of the RNA-protein
602 interactions. Six replications were carried out for each treatment.
603
604 **Feeding treatment of agomir-252 and antagomir-252**
605 To determine the effect of miR-252 on *CcTRPM* expression, summer-form 1st instar nymphs
606 were fed with agomir-252 (1 μM) or antagomir-252 (1 μM) and collected at 6 d after treatment for
607 qRT-PCR. Agomir/antagomir negative control was fed as the control. To test the effect of
608 miR-252 on the transition of summer-form to winter-form, summer-form 1st instar nymphs were
609 fed with agomir-252 (1 μM) or agomir-NC (1 μM) and divided into three groups. (1) The samples
610 were collected after different agomir feeding at 3 d and 6 d under 10°C condition, then for
611 miR-252 expression analysis using qRT-PCR. (2) The samples were collected after agomir
612 feeding at 12 d for cuticle ultrastructure comparison, cuticle chitin staining with WGA-FITC, and
613 determination of cuticle chitin content under 10°C condition according to the above methods. (3)
614 Observed the morphological characteristics every two days and counted the number of
615 summer-form and winter-form individuals based on the above description until the 3rd instar
616 under 10°C condition.
617 For the rescue by antagomir-252 feeding under dsCcTRPM treatment, summer-form 1st
618 instar nymphs were fed with the mixture of antagomir-252 (1 μM) and dsCcTRPM (500 ng/μL),
619 then counted the number of summer-form and winter-form individuals based the above method
620 until the 3rd instar under 10°C condition. All the experiments were performed in nine replications
621 with at least 30 nymphs for each replication.
622
623 **Statistical analysis**
624 GraphPad Prism 8.0 software and IBM SPSS Statistics 26.0 were used for making figures
625 and statistical analysis, respectively. All the data were shown as means ± standard deviation (SD)
626 with different independent biological replications. Student's *t*-test was performed for pairwise
627 comparisons to determine the statistically significant differences between treatments and controls
628 (***$P < 0.001$). One-way ANOVA followed by the Tukey's HSD multiple comparison test was
629 used for multiple comparisons (different letters denoted by $P < 0.05$).
630
631 **Acknowledgements**
632 Thanks for the funding support by the National Natural Science Foundation of China (32202291)
633 and China Agriculture Research System (CARS-28).
634
635 **Authors' contributions**

S.Z., and X.L. designed research; S.Z., J.L., and D.Z. performed research; Z.Z., and S.M. contributed new analytic tools; S.Z., J.L., D.Z., Z.Z., S.M., and Z.L. analyzed data; S.Z. wrote the paper; and S.Z., and X.L. provided the fund.

Data accessibility

The published article includes all data generated or analyzed during this study. The full sequences were submitted to NCBI, accession number: OQ658558 for *CcTRPM*, OQ734934 for *CcTre1*, and OQ658570 for *CcCHS1*.

Funding

This work was funded by the National Natural Science Foundation of China (32202291) and China Agriculture Research System (CARS-28).

Competing interests

The authors declared no competing financial interests.

References

Agarwal, V., Bell, G. W., Nam, J.W., & Bartel, D. P. (2015). Predicting effective microRNA target sites in mammalian mRNAs. *ELife*, *4*, e05005. https://doi.org/10.7554/eLife.05005

An, C., Fei, X., Chen, W., & Zhao, Z. (2012). The integrative effects of population density, photoperiod, temperature, and host plant on the induction of alate aphids in *Schizaphis graminum*. *Archives of Insect Biochemistry and Physiology*, *79*(4–5), 198–206. https://doi.org/10.1002/arch.21005

Asgari, S. (2013). MicroRNA functions in insects. *Insect Biochemistry and Molecular Biology*, *43*(4), 388–397. https://doi.org/10.1016/j.ibmb.2012.10.005

Butt, B. A., & Stuart, C. (1986). Oviposition by summer and winter forms of *Pear Psylla* (Homoptera: Psyllidae) on dormant pear budwood. *Environmental Entomology*, *5*, 1109–1110. https://doi.org/10.1093/ee/15.5.1109

Chen, S., Nichols, K. M., Poynton, H. C., & Sepúlveda, M. S. (2016). MicroRNAs are involved in cadmium tolerance in *Daphnia pulex*. *Aquatic Toxicology (Amsterdam, Netherlands)*, *175*, 241–248. https://doi.org/10.1016/j.aquatox.2016.03.023

Cridge, A. G., Leask, M. P., Duncan, E. J., & Dearden, P. K. (2015). What do studies of insect polyphenisms tell us about nutritionally-triggered epigenomic changes and their consequences? *Nutrients*, *7*(3), 1787–1797. https://doi.org/10.3390/nu7031787

Dai, T.M., Wang, Y.S., Liu, W.X., Lü, Z.C., & Wan, F.H. (2018). Thermal discrimination and transgenerational temperature response in *Bemisia tabaci* Mediterranean (Hemiptera: Aleyrodidae): putative involvement of the thermo-sensitive receptor *BtTRPA*. *Environmental Entomology*, *47*(1), 204–209. https://doi.org/10.1093/ee/nvx202

Ekino, T., Yoshiga, T., Takeuchi-Kaneko, Y., & Kanzaki, N. (2017). Transmission electron microscopic observation of body cuticle structures of phoretic and parasitic stages of Parasitaphelenchinae nematodes. *PloS One*, *12*(6), e0179465. https://doi.org/10.1371/journal.pone.0179465

Enright, A. J., John, B., Gaul, U., Tuschl, T., Sander, C., & Marks, D. S. (2003). MicroRNA targets in *Drosophila*. *Genome Biology*, *5*(1), R1. https://doi.org/10.1186/gb-2003-5-1-r1

Evans, A. R., & Sanson, G. D. (2005). Biomechanical properties of insects in relation to insectivory: Cuticle thickness as an indicator of insect “hardness” and “intractability.” *Australian Journal of Zoology*, *53*(1), 9–19. https://doi.org/10.1071/zo04018

Farnesi, L. C., Brito, J. M., Linss, J. G., Pelajo-Machado, M., Valle, D., & Rezende, G. L. (2012). Physiological and morphological aspects of *Aedes aegypti* developing larvae: effects of the chitin synthesis inhibitor novaluron. *PLoS ONE*, *7*(1), e30363. https://doi.org/10.1371/journal.pone.0030363

Fedorka, K. M., Copeland, E. K., & Winterhalter, W. E. (2013). Seasonality influences cuticle melanization and immune defense in a cricket: support for a temperature-dependent immune investment hypothesis in insects. *The Journal of Experimental Biology*, *216*(Pt 21), 4005–4010. https://doi.org/10.1242/jeb.091538

Fu, T., Hull, J. J., Yang, T., & Wang, G. (2016). Identification and functional characterization of four transient receptor potential ankyrin 1 variants in *Apolygus lucorum* (Meyer-Dür). *Insect Molecular Biology*, *25*(4), 370–384. https://doi.org/10.1111/imb.12231

Ge, Y., Zhang, L., Qin, Z., Wang, Y., Liu, P., Tan, S., Fu, Z., Smith, O. M., & Shi, W. (2019). Different predation capacities and mechanisms of *Harmonia axyridis* (Coleoptera: Coccinellidae) on two morphotypes of pear psylla *Cacopsylla chinensis* (Hemiptera: Psyllidae). *PLoS ONE*, *14*(4), e0215834. https://doi.org/10.1371/journal.pone.0215834

Guo, S., Tian, Z., Wu, Q.W., King-Jones, K., Liu, W., Zhu, F., & Wang, X.P. (2021). Steroid hormone ecdysone deficiency stimulates preparation for photoperiodic reproductive diapause. *PLoS Genetics*, *17*(2), e1009352. https://doi.org/10.1371/journal.pgen.1009352

Hildebrand, M., Dickler, E., & Geider, K. (2010). Occurrence of *Erwinia amylovora* on insects in a fire blight orchard. *Journal of Phytopathology*, *148*(4), 251–256. https://doi.org/10.1046/j.1439-0434.2000.00504.x

Hou, L., Yang, P., Jiang, F., Liu, Q., Wang, X., & Kang, L. (2017). The neuropeptide F/nitric oxide pathway is essential for shaping locomotor plasticity underlying locust phase transition. *ELife*, *6*, e22526. https://doi.org/10.7554/eLife.22526

Kennell, J. A., Cadigan, K. M., Shakhmantsir, I., & Waldron, E. J. (2012). The microRNA miR-8 is a positive regulator of pigmentation and eclosion in *Drosophila*. *Developmental Dynamics: An Official Publication of the American Association of Anatomists*, *241*(1), 161–168. https://doi.org/10.1002/dvdy.23705

Kliot, A., Kontsedalov, S., Lebedev, G., Brumin, M., Cathrin, P. B., Marubayashi, J. M., Skaljac, M., Belausov, E., Czosnek, H., & Ghanim, M. (2014). Fluorescence in situ hybridizations (FISH) for the localization of viruses and endosymbiotic bacteria in plant and insect tissues. *Journal of Visualized Experiments: JoVE*, *84*, 51030. https://doi.org/10.3791/51030

Kreß, A., Kuch, U., Oehlmann, J., & Müller, R. (2016). Effects of diapause and cold acclimation on egg ultrastructure: new insights into the cold hardiness mechanisms of the Asian tiger mosquito *Aedes (Stegomyia) albopictus*. *Journal of Vector Ecology: Journal of the Society for Vector Ecology*, *41*(1), 142–150. https://doi.org/10.1111/jvec.12206

Lee, Y., Lee, Y., Lee, J., Bang, S., Hyun, S., Kang, J., Hong, S.T., Bae, E., Kaang, B.K., & Kim, J. (2005). Pyrexia is a new thermal transient receptor potential channel endowing tolerance to high temperatures in *Drosophila melanogaster*. *Nature Genetics*, *37*(3), 305–310. https://doi.org/10.1038/ng1513

Liu, F., Peng, W., Li, Z., Li, W., Li, L., Pan, J., Zhang, S., Miao, Y., Chen, S., & Su, S. (2012). Next-generation small RNA sequencing for microRNAs profiling in *Apis mellifera*: Comparison between nurses and foragers. *Insect Molecular Biology*, *21*(3), 297–303. https://doi.org/10.1111/j.1365-2583.2012.01135.x

Livak, K. J., & Schmittgen, T. D. (2001). Analysis of relative gene expression data using real-time quantitative PCR and the $2^{-\Delta\Delta CT}$ method. *Methods*, *25*(4), 402–408. https://doi.org/10.1006/meth.2001.1262

Lyons, P. J., Crapoulet, N., Storey, K. B., & Morin, P. (2015). Identification and profiling of miRNAs in the freeze-avoiding gall moth *Epiblema scudderiana* via next-generation sequencing. *Molecular and Cellular Biochemistry*, *410*(1–2), 155–163. https://doi.org/10.1007/s11010-015-2547-3

Ma, Z., Guo, W., Guo, X., Wang, X., & Kang, L. (2011). Modulation of behavioral phase changes of the migratory locust by the catecholamine metabolic pathway. *Proceedings of the*

National Academy of Sciences of the United States of America, *108*(10), 3882–3887. https://doi.org/10.1073/pnas.1015098108

McKemy, D. D., Neuhausser, W. M., & Julius, D. (2002). Identification of a cold receptor reveals a general role for TRP channels in thermosensation. *Nature*, *416*(6876), 52–58. https://doi.org/10.1038/nature719

Minke, B., Wu, C., & Pak, W. L. (1975). Induction of photoreceptor voltage noise in the dark in *Drosophila* mutant. *Nature*, *258*(5530), 84–87. https://doi.org/10.1038/258084a0

Morin, M. D., Frigault, J. J., Lyons, P. J., Crapoulet, N., Boquel, S., Storey, K. B., & Morin, P. J. (2017). Amplification and quantification of cold-associated microRNAs in the Colorado potato beetle (*Leptinotarsa decemlineata*) agricultural pest. *Insect Molecular Biology*, *26*(5), 574–583. https://doi.org/10.1111/imb.12320

Neely, G. G., Keene, A. C., Duchek, P., Chang, E. C., Wang, Q.P., Aksoy, Y. A., Rosenzweig, M., Costigan, M., Woolf, C. J., Garrity, P. A., & Penninger, J. M. (2011). TrpA1 regulates thermal nociception in *Drosophila*. *PloS One*, *6*(8), e24343. https://doi.org/10.1371/journal.pone.0024343

Oldfield, & G., N. (1970). Diapause and polymorphism in california populations of *Psylla pyricola* (Homoptera: Psyllidae). *Annals of the Entomological Society of America*, *63*(1), 180–184. https://doi.org/10.1093/aesa/63.1.180

Peier, A. M., Moqrich, A., Hergarden, A. C., Reeve, A. J., Andersson, D. A., Story, G. M., Earley, T. J., Dragoni, I., McIntyre, P., Bevan, S., & Patapoutian, A. (2002). A TRP channel that senses cold stimuli and menthol. *Cell*, *108*(5), 705–715. https://doi.org/10.1016/S0092-8674(02)00652-9

Richards, A. G. (1978). The chemistry of insect cuticle. *Biochemistry of Insects*, 205–232. https://doi.org/10.1016/B978-0-12-591640-0.50010-8

Rosenzweig, M., Kang, K., & Garrity, P. A. (2008). Distinct TRP channels are required for warm and cool avoidance in *Drosophila melanogaster*. *Proceedings of the National Academy of Sciences of the United States of America*, *105*(38), 14668–14673. https://doi.org/10.1073/pnas.0805041105

Sato, A., Sokabe, T., Kashio, M., Yasukochi, Y., Tominaga, M., & Shiomi, K. (2014). Embryonic thermosensitive TRPA1 determines transgenerational diapause phenotype of the silkworm, *Bombyx mori*. *Proceedings of the National Academy of Sciences of the United States of America*, *111*(13), E1249–E1255. https://doi.org/10.1073/pnas.1322134111

Shang, F., Niu, J., Ding, B.Y., Zhang, W., Wei, D.D., Wei, D., Jiang, H.B., & Wang, J.J. (2020). The miR-9b microRNA mediates dimorphism and development of wing in aphids. *Proceedings of the National Academy of Sciences*, *117*(15), 8404–8409. https://doi.org/10.1073/pnas.1919204117

Shiels, A. (2020). TRPM3_miR-204: A complex locus for eye development and disease. *Human Genomics*, *14*(1), 7. https://doi.org/10.1186/s40246-020-00258-4

Simpson, S. J., Sword, G. A., & Lo, N. (2011). Polyphenism in insects. *Current Biology*, *21*(18), R738–R749. https://doi.org/10.1016/j.cub.2011.06.006

Teets, N. M., Marshall, K. E., & Reynolds, J. A. (2023). Molecular mechanisms of winter survival. *Annual Review of Entomology*, *68*, 319–339. https://doi.org/10.1146/annurev-ento-120120-095233

Terblanche, J. S., Hoffmann, A. A., Mitchell, K. A., Rako, L., le Roux, P. C., & Chown, S. L. (2011). Ecologically relevant measures of tolerance to potentially lethal temperatures. *The Journal of Experimental Biology*, *214*(Pt 22), 3713–3725. https://doi.org/10.1242/jeb.061283

Tougeron, K., Iltis, C., Renoz, F., Albittar, L., Hance, T., Demeter, S., & Le Goff, G. J. (2021). Ecology and biology of the parasitoid *Trechnites insidiosus* and its potential for biological control of pear psyllids. *Pest Management Science*, *77*(11), 4836–4847. https://doi.org/10.1002/ps.6517

Tracey, W. D., Wilson, R. I., Laurent, G., & Benzer, S. (2003). Painless, a *Drosophila* gene essential for nociception. *Cell*, *113*(2), 261–273. https://doi.org/10.1016/s0092-8674(03)00272-1

Tsuchiya, R., Kaneshima, A., Kobayashi, M., Yamazaki, M., Takasu, Y., Sezutsu, H., Tanaka, Y., Mizoguchi, A., & Shiomi, K. (2021). Maternal GABAergic and GnRH/corazonin pathway modulates egg diapause phenotype of the silkworm Bombyx mori. *Proceedings of the National Academy of Sciences of the United States of America*, *118*(1), e2020028118. https://doi.org/10.1073/pnas.2020028118

Turner, H. N., Armengol, K., Patel, A. A., Himmel, N. J., Sullivan, L., Iyer, S. C., Bhattacharya, S., Iyer, E. P. R., Landry, C., Galko, M. J., & Cox, D. N. (2016). The TRP channels Pkd2, NompC and Trpm act in cold-sensing neurons to mediate unique aversive behaviors to noxious cold in Drosophila. *Current Biology: CB*, *26*(23), 3116–3128. https://doi.org/10.1016/j.cub.2016.09.038

Vargas, H. C. M., Farnesi, L. C., Martins, A. J., Valle, D., & Rezende, G. L. (2014). Serosal cuticle formation and distinct degrees of desiccation resistance in embryos of the mosquito vectors Aedes aegypti, Anopheles aquasalis and Culex quinquefasciatus. *Journal of Insect Physiology*, *62*, 54–60. https://doi.org/10.1016/j.jinsphys.2014.02.001

Vellichirammal, N. N., Gupta, P., Hall, T. A., & Brisson, J. A. (2017). Ecdysone signaling underlies the pea aphid transgenerational wing polyphenism. *Proceedings of the National Academy of Sciences of the United States of America*, *114*(6), 1419–1423. https://doi.org/10.1073/pnas.1617640114

Venkatachalam, K., & Montell, C. (2007). TRP channels. *Annual Review of Biochemistry*, *76*, 387–417. https://doi.org/10.1146/annurev.biochem.75.103004.142819

Wang, L.-X., Niu, C.-D., Wu, S.-F., & Gao, C.-F. (2021). Molecular characterizations and expression profiles of transient receptor potential channels in the brown planthopper, Nilaparvata lugens. *Pesticide Biochemistry and Physiology*, *173*, 104780. https://doi.org/10.1016/j.pestbp.2021.104780

Wang, X.-D., Lin, Z.-K., Ji, S.-X., Bi, S.-Y., Liu, W.-X., Zhang, G.-F., Wan, F.-H., & Lü, Z.-C. (2021). Molecular characterization of TRPA subfamily genes and function in temperature preference in *Tuta absoluta* (Meyrick) (Lepidoptera: Gelechiidae). *International Journal of Molecular Sciences*, *22*(13), 7157. https://doi.org/10.3390/ijms22137157

Wei, M., Chi, H., Guo, Y., Li, X., Zhao, L., & Ma, R. (2020). Demography of *Cacopsylla chinensis* (Hemiptera: Psyllidae) reared on four cultivars of *Pyrus bretschneideri* (Rosales: Rosaceae) and *P. communis* Pears with estimations of confidence intervals of specific life table statistics. *Journal of Economic Entomology*, *113*(5), 2343–2353. https://doi.org/10.1093/jee/toaa149

Xie, J., Peng, G., Wang, M., Zhong, Q., Song, X., Bi, J., Tang, J., Feng, F., Gao, H., & Li, B. (2022). RR-1 cuticular protein TcCPR69 is required for growth and metamorphosis in *Tribolium castaneum*. *Insect Science*, *29*(6), 1612–1628. https://doi.org/10.1111/1744-7917.13038

Xu, H.J., Xue, J., Lu, B., Zhang, X.C., Zhuo, J.C., He, S.F., Ma, X.F., Jiang, Y.Q., Fan, H.W., Xu, J.Y., Ye, Y.X., Pan, P.L., Li, Q., Bao, Y.Y., Nijhout, H. F., & Zhang, C.X. (2015). Two insulin receptors determine alternative wing morphs in planthoppers. *Nature*, *519*(7544), 464–467. https://doi.org/10.1038/nature14286

Yang, M., Wei, Y., Jiang, F., Wang, Y., Guo, X., He, J., & Kang, L. (2014). MicroRNA-133 inhibits behavioral aggregation by controlling dopamine synthesis in Locusts. *PLoS Genetics*, *10*(2), e1004206. https://doi.org/10.1371/journal.pgen.1004206

Yang, S., Zhang, J., Wang, S., Zhang, X., Liu, Y., & Xi, J. (2017). Identification and profiling of miRNAs in overwintering *Lissorhoptrus oryzophilus* via next-generation sequencing. *Cryobiology*, *74*, 68–76. https://doi.org/10.1016/j.cryobiol.2016.11.013

Yang, X., Wu, D., Du, H., Nie, F., Pang, X., & Xu, Y. (2017). MicroRNA-135a is involved in podocyte injury in a transient receptor potential channel 1-dependent manner. *International Journal of Molecular Medicine*, *40*(5), 1511–1519. https://doi.org/10.3892/ijmm.2017.3152

Ye, X., Xu, L., Li, X., He, K., Hua, H., Cao, Z., Xu, J., Ye, W., Zhang, J., Yuan, Z., & Li, F. (2019). MiR-34 modulates wing polyphenism in planthopper. *PLoS Genetics*, *15*(6), e1008235. https://doi.org/10.1371/journal.pgen.1008235

Zhang, B., Zhao, L., Ning, J., Wickham, J. D., Tian, H., Zhang, X., Yang, M., Wang, X., & Sun, J. (2020). MiR-31-5p regulates cold acclimation of the wood-boring beetle *Monochamus alternatus* via ascaroside signaling. *BMC Biology*, *18*(1), 184. https://doi.org/10.1186/s12915-020-00926-w

Zhang, J.L., Chen, S.J., Liu, X.Y., Moczek, A. P., & Xu, H.J. (2022). The transcription factor Zfh1 acts as a wing-morph switch in planthoppers. *Nature Communications*, *13*(1), 5670. https://doi.org/10.1038/s41467-022-33422-6

853 **Figure legends**

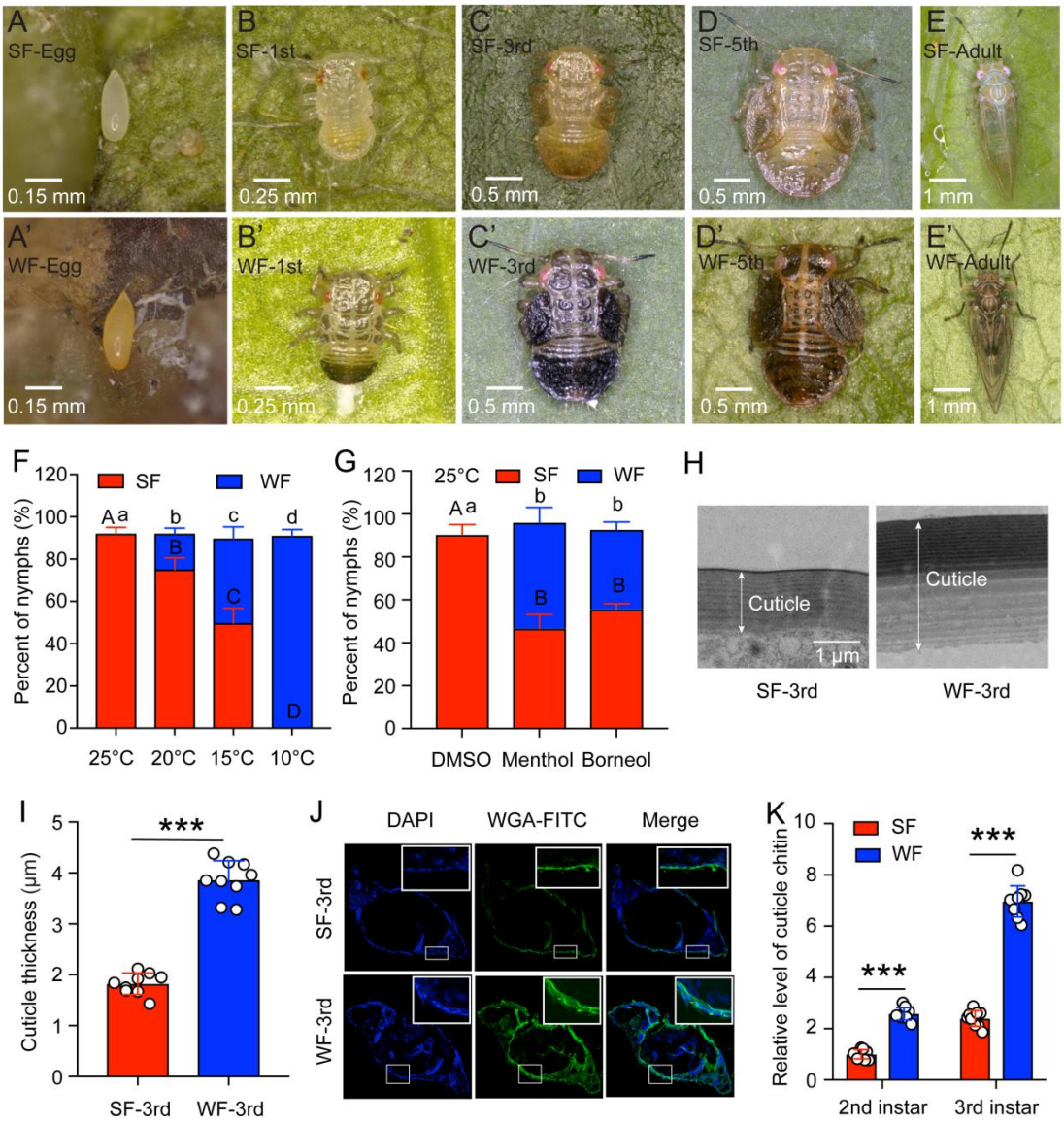

854

855 **Figure 1. Low temperature induced the transition from summer form (SF) to winter form**
856 **(WF) in *C. chinensis*.**

857 A-E and A'-E': The morphology of egg, 1st, 3rd, and 5th instar nymph, 5 days adult for SF and
858 WF of *C. chinensis*, respectively. The scale bars were labeled in the lower left of each figure.

859 F: Percent of SF and WF under different temperatures (25°C, 20°C, 15°C, and 10°C) when
860 induction of newly-hatched (within 12 h) 1st instar nymph of *C. chinensis*.

861 G: Effect of two chemical cooling agents (menthol and borneol) on the percent of SF and WF
862 when induction of newly-hatched (within 12 h) 1st instar nymph of *C. chinensis* under 25°C.

863 H: Ultrastructure comparison of the nymph cuticle for SF 3rd instar and WF 3rd instar of *C.*
864 *chinensis* using transmission electron microscopy. Scale bar is 1 μm. The two-way arrow
865 indicated the cuticle thickness.

866 I: Comparison of the nymph cuticle thickness for SF 3rd instar and WF 3rd instar of *C. chinensis*.

867 J: Chitin staining of nymph cuticle with WGA-FITC in SF 3rd instar and WF 3rd instar of *C.*

868 *chinensis*. DAPI: the cell nuclei were stained with DAPI and visualized in blue. WAG-FITC: the
869 cuticle chitin was labeled with FITC and visualized in green. Merge: merged imaging of DAPI,
870 and WAG-FITC signals.
871 K: Determination of cuticle chitin content in 2nd and 3rd instar nymph of SF and WF.
872 The data of nymph percent were shown as the mean ± SD with three independent biological
873 replications of at least 30 nymphs for each biological replication. Different letters above the bars
874 indicated statistically significant differences ($p < 0.05$), as determined by ANOVA followed with
875 a Turkey's HSD multiple comparison test in SPSS 20.0 software. The results of cuticle thickness
876 and cuticle chitin content were presented as mean ± SD of three independent biological samples
877 with three technical replications for each biological replication. Statistically significant differences
878 were determined with the pair-wise Student's *t*-test, and significance levels were denoted by *** (p
879 < 0.001).
880

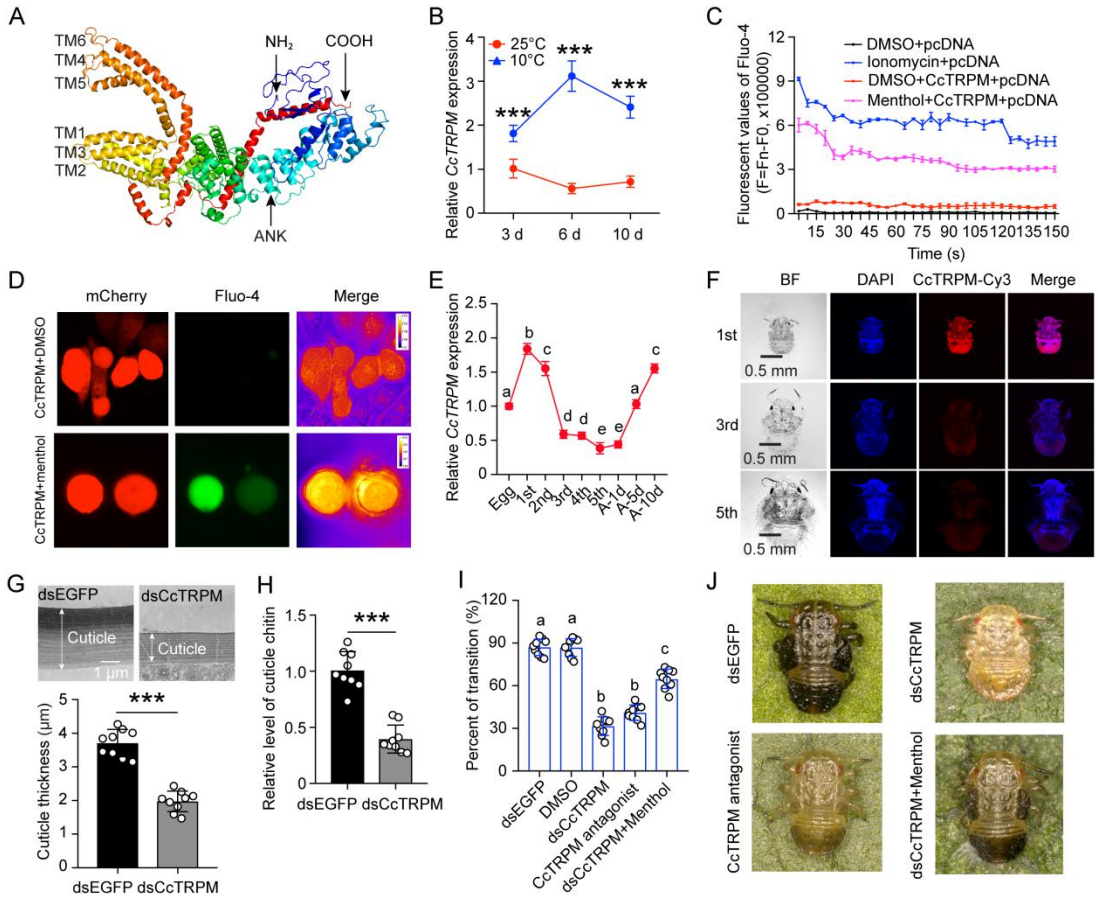

881
882 **Figure 2. Temperature receptor *CcTRPM* modulated the transition from SF to WF of *C.***
883 ***chinensis* in response to low temperature.**
884 A: The predicted protein tertiary structure of *CcTRPM*. The conserved ankyrin repeat (ANK)
885 domain was indicated in the N-terminal. The conserved six transmembrane domain of ion
886 channels structure were shown as TM1-TM6.
887 B: The mRNA expression of *CcTRPM* in response to different temperatures of 25°C and 10°C by
888 qRT-PCR.
889 C: Fluorescence detection of Fluo-4 AM after heterologous expression of *CcTRPM* in mammalian
890 HEK293T cells in response to menthol treatment. The recombinant plasmid was generated by

891 inserting the full ORF sequence of *CcTRPM* into pcDNA3.1(+)-mCherry plasmid. DMSO
892 treatment and ionomycin treatment were used as negative control and positive control, separately.
893 D: Representative images of Ca^{2+} imaging after heterologous expression of *CcTRPM* in
894 mammalian HEK293T cells in response to menthol treatment. CcTRPM (+) means the
895 recombinant plasmid of *CcTRPM* with pcDNA3.1(+)-mCherry. CcTRPM (-) denotes the
896 pcDNA3.1(+)-mCherry plasmid without *CcTRPM*. mCherry and Fluo-4 signal are shown in red
897 and green, respectively.
898 E: The developmental expression pattern of *CcTRPM* for SF at mRNA level using qRT-PCR. 1st,
899 2nd, 3rd, 4th and 5th are the nymphs at the first, second, third, fourth and fifth instar, respectively.
900 A-1d, A-5d, and A-10d are the adults at 1 day, 5 days, and 10 days, separately.
901 F: Representative confocal images of *CcTRPM* in different developmental stages of SF using
902 FISH. Scale bar is 0.5 mm. BF: the bright field. DAPI: the cell nuclei were stained with DAPI and
903 visualized in blue. CcTRPM-Cy3: CcTRPM signal was labeled with Cy3 and visualized in red.
904 Merge: merged imaging of BF, DAPI, and CcTRPM-Cy3 signals.
905 G-H: Comparison of the nymph cuticle ultrastructure, cuticle thickness, and cuticle chitin content
906 of SF 1st instar treated with dsCcTRPM and dsEGFP at 15 d.
907 I: The transition percent of SF 1st instar nymphs treated with dsEGFP, DMSO, dsCcTRPM,
908 CcTRPM antagonist and dsCcTRPM+menthol at 15 d under 10°C.
909 J: The phenotypes of SF 1st instar nymphs treated with dsEGFP, dsCcTRPM, CcTRPM antagonist
910 and dsCcTRPM+menthol at 15 d under 10°C.
911 The data in 2B and 2E are shown as the mean ± SD with three independent biological replications
912 of at least 30 nymphs for each biological replication. Data in 2G and 2H are presented as mean ±
913 SD with three biological replications of three technical replicates for each biological replication.
914 Data in 2I are presented as mean ± SD with nine biological replications. Statistically significant
915 differences were determined with the pair-wise Student's *t*-test, and significance levels were
916 denoted by *** ($p < 0.001$). Different letters above the bars indicated statistically significant
917 differences ($p < 0.05$), as determined by ANOVA followed with a Turkey's HSD multiple
918 comparison test in SPSS 20.0 software.
919

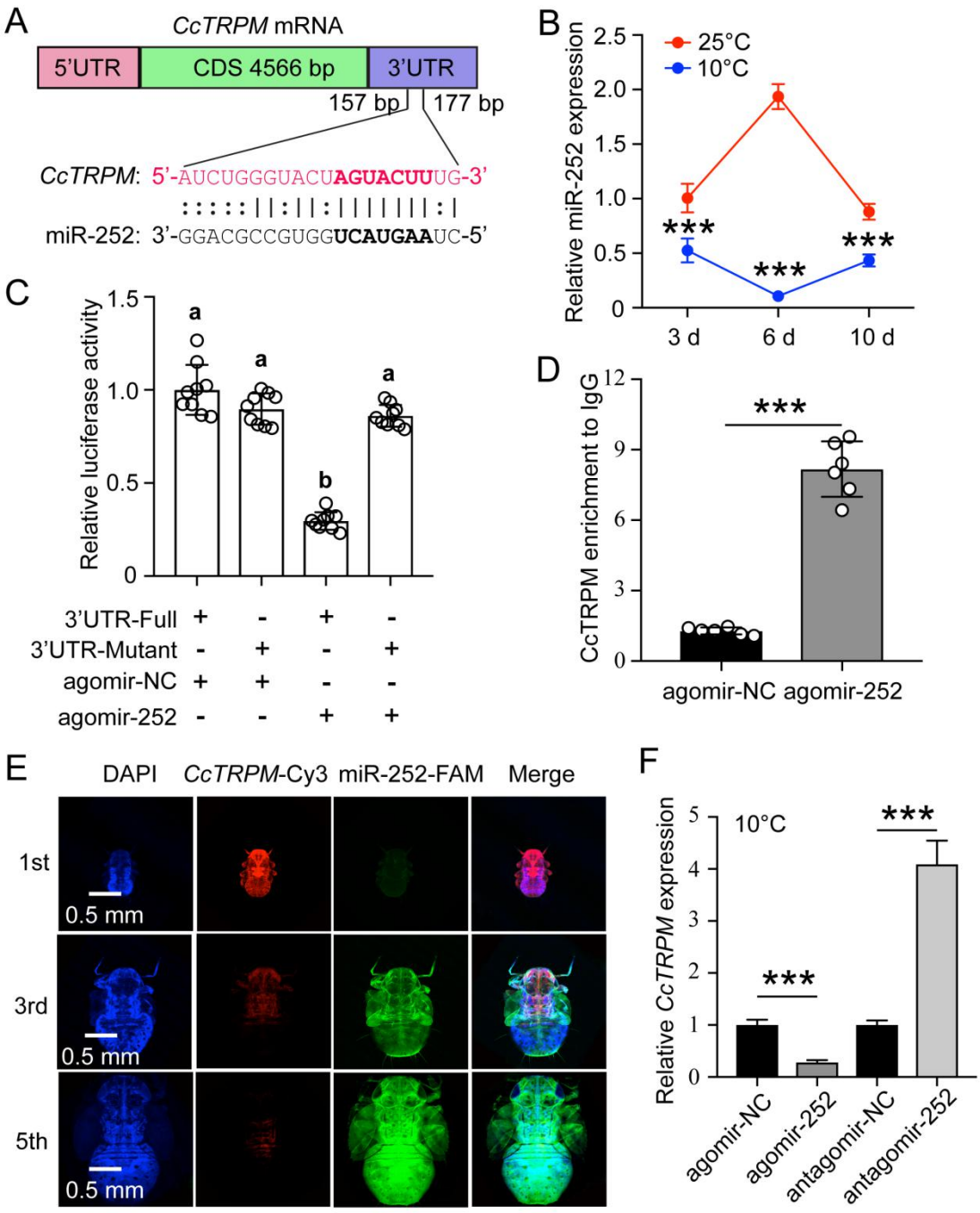

Figure 3. Confirming of miR-252 targeted *CcTRPM*.

A: The putative miR-252 binding sites in *CcTRPM* 3'UTR were predicted by miRanda and Targetscan.

B: The expression profiles of miR-252 in response to different temperatures of 25°C and 10°C by qRT-PCR.

C: In vitro validation of the target interactions between miR-252 and *CcTRPM* by dual luciferase reporter assays.

D: In vivo demonstration of miR-252 targeting *CcTRPM* by RNA-binding protein immunoprecipitation (RIP) assay.

E: Representative confocal images of miR-252 and *CcTRPM* in 1st, 3rd and 5th instar of SF. Scale bar is 0.5 mm. The signals of DAPI and *CcTRPM*-Cy3 are same as the above describing.

932 miR-252-FAM: the miR-252 signal was labeled with FAM and visualized in green. Merge:
933 merged imaging of co-localization of cell nucleus, *CcTRPM* and miR-252.
934 F: Effect of miR-252 agomir and antagomir treatment 3 days on the expression of *CcTRPM* at
935 mRNA level.
936 The data in 3B and 3F are shown as the mean ± SD with three independent biological replications
937 of at least 30 nymphs for each biological replication. Data in 3C are presented as mean ± SD with
938 nine biological replications. Data in 3D are presented as mean ± SD with two biological
939 replications of three technical replicates for each biological replication. Statistically significant
940 differences were determined with the pair-wise Student's *t*-test, and significance levels were
941 denoted by *** ($p < 0.001$). Different letters above the bars indicated statistically significant
942 differences ($p < 0.05$), as determined by ANOVA followed with a Turkey's HSD multiple
943 comparison test in SPSS 20.0 software.
944

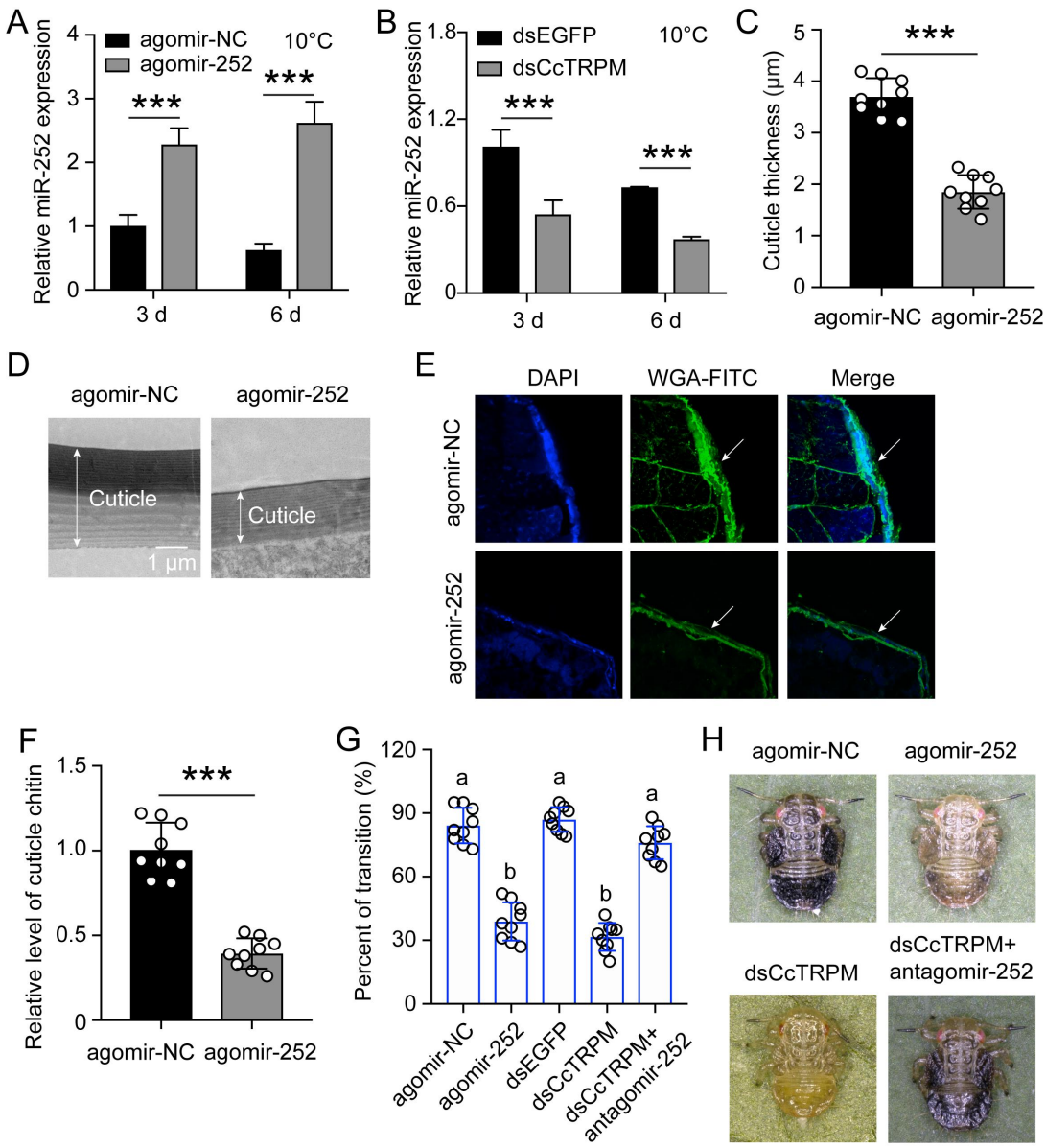

945
946 **Figure 4. miR-252 mediated the transition from SF to WF in *C. chinensis* by suppressing**

947 ***CcTRPM.***
948 A: Effect of miR-252 agomir treatment on the mRNA expression of miR-252 after 3 d and 6 d
949 under 10°C. agomir-NC treatment was used as the control. 3 d: 3 days. 6 d: 6 days.
950 B: The mRNA expression of miR-252 after dsCcTRPM treatment 3 d and 6 d compare with the
951 dsEGFP treatment under 10°C.
952 C-F: Comparison of the nymph cuticle thickness, cuticle ultrastructure, cuticle chitin staining with
953 WGA-FITC, and chitin content of SF 1st instar after treatment with agomir-NC and agomir-252 at
954 15 d. Scale bar is 1 μm. The two-way arrow indicated the cuticle thickness. The DAPI and
955 WAG-FITC signals were same as the above describing.
956 G: The transition percent of SF 1st instar nymphs treated with agomir-NC, agomir-252, dsEGFP,
957 dsCcTRPM, and dsCcTRPM+antagomir-252 at 15 d under 10°C.
958 H: The phenotypes of SF 1st instar nymphs treated with agomir-NC, agomir-252, dsCcTRPM, and
959 dsCcTRPM+antagomir-252 at 15 d under 10°C.
960 The data in 4A and 4B are shown as the mean ± SD with three independent biological replications
961 of at least 30 nymphs for each biological replication. Data in 4C and 4F are presented as mean ±
962 SD with three biological replications of three technical replications for each biological replication.
963 Data in 4G are presented as mean ± SD with nine biological replications. Statistically significant
964 differences were determined with the pair-wise Student's *t*-test, and significance levels were
965 denoted by *** ($p < 0.001$). Different letters above the bars indicated statistically significant
966 differences ($p < 0.05$), as determined by ANOVA followed with a Turkey's HSD multiple
967 comparison test in SPSS 20.0 software.
968

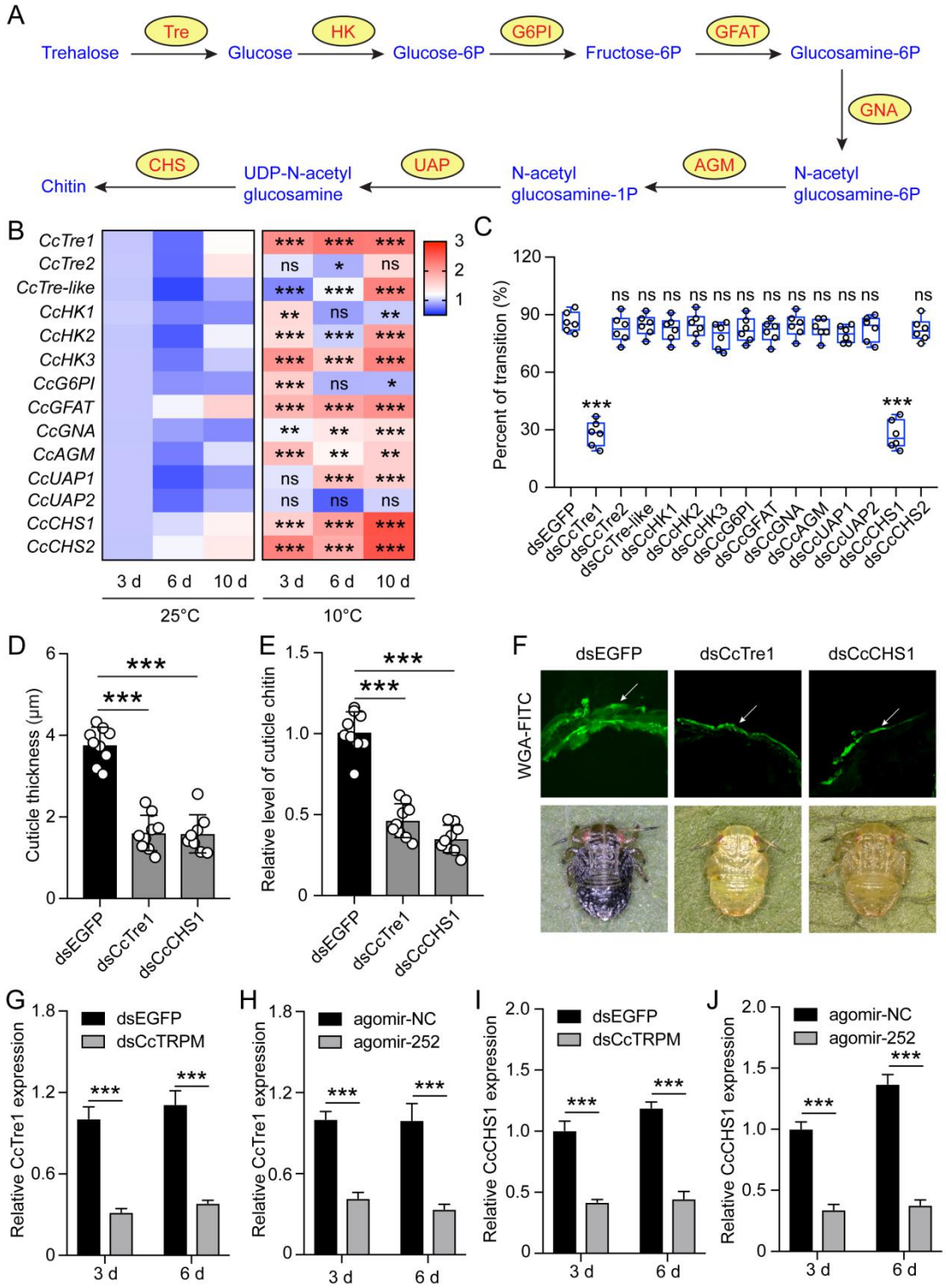

969

970 **Figure 5. Chitin biosynthesis signaling involved in the transition from SF to WF of *C.***
971 ***chinensis* in response to low temperature and *CcTRPM*.**

972 A: Diagram of de novo biosynthesis of insect chitin. Tre: trehalase. HK: hexokinase. G6PI:
973 glucose-6-phosphate isomerase. GFAT: fructose-6-phosphate aminotransferase. GNA:
974 glucosamine-6-phosphate acetyltransferase. AGM: N-acetylglucosamine phosphate mutase. UAP:
975 UDP- N-acetylglucosamine pyrophosphorylase. CHS: chitin synthase.

976 B: A heat map was constructed from the expression levels of chitin biosynthesis enzyme

transcripts in *C. chinensis* after 25°C and 10°C treatment at 3 d, 6 d, and 10 d.

C: Effect of RNAi knockdown of 14 transcripts covering all the enzymes in the chitin biosynthesis pathway on the transition percent of SF 1st instar nymphs under 10°C.

D-F: Comparison of the nymph cuticle thickness, cuticle chitin content, and cuticle chitin staining with WGA-FITC of SF 1st instar after treatment with dsEGFP, dsCcTre1, and dsCcCHS1 at 15 d. The WAG-FITC signal was same as the above describing.

G-H: Effect of dsCcTRPM and agomir-252 treatments on the mRNA expression of *CcTre1* at 3 d and 6 d under 10°C.

I-J: Effect of dsCcTRPM and agomir-252 treatments on the mRNA expression of *CcCHS1* at 3 d and 6 d under 10°C.

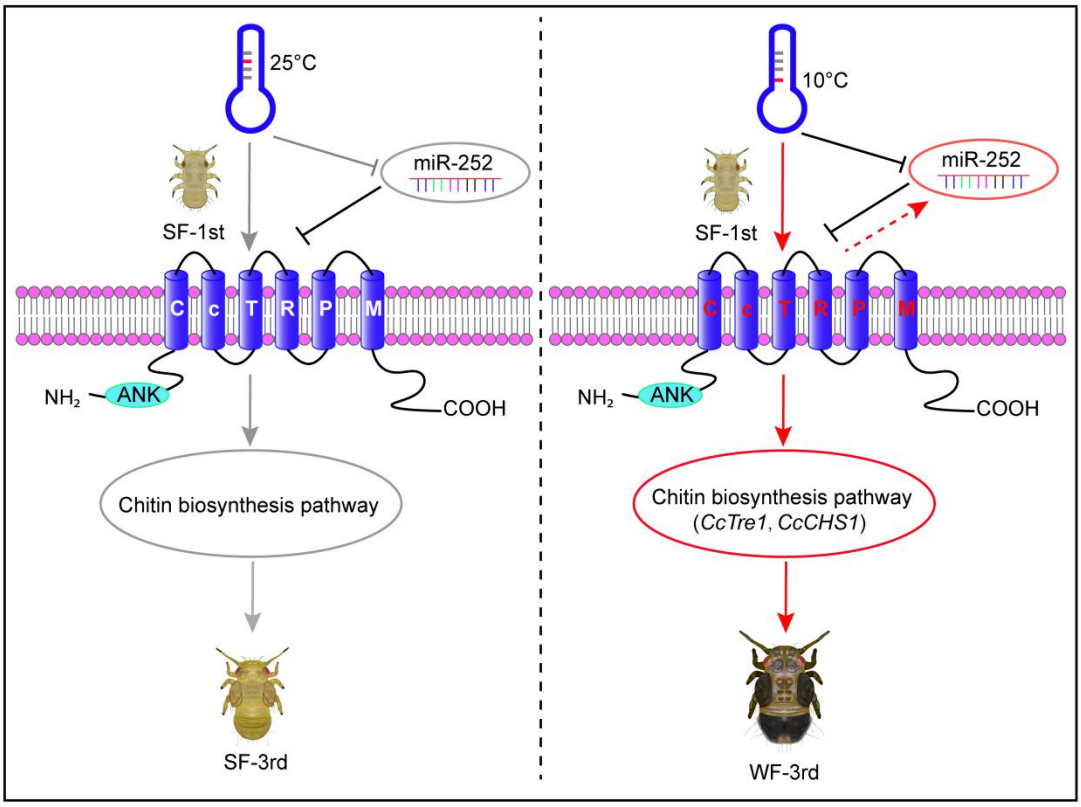

Figure 6. A model showing the key roles of miR-252 targeting *CcTRPM* to regulate the transition from SF to WF of *C. chinensis* in response to low temperature.

Under 25°C condition, the temperature receptor *CcTRPM* was inactive as inhibiting by miR-252 in 1st instar nymphs of SF. The 1st instar nymphs of SF normally developed into 3rd instar nymphs of SF. However, under 10°C condition, low temperature profoundly activated *CcTRPM* expression, miR-252 functioned as a negative regulator to mediate the expression of *CcTRPM* in case of over-expression in response to low temperature. Then, *CcTRPM* significantly increased the activity of chitin biosynthesis pathway, especially *CcTre1* and *CcCHS1*, and led to cuticle chitin content was obvious raise and cuticle thickness became thicker. Finally, the 1st instar nymphs of SF developed to 3rd instar nymphs of WF in order to better adapt to low temperature. Red arrows and black T-bars indicated the activation and inhibition, respectively. Gray arrows and T-bars represented the inactive states of the genes or physiological processes, separately.

Supplemental information

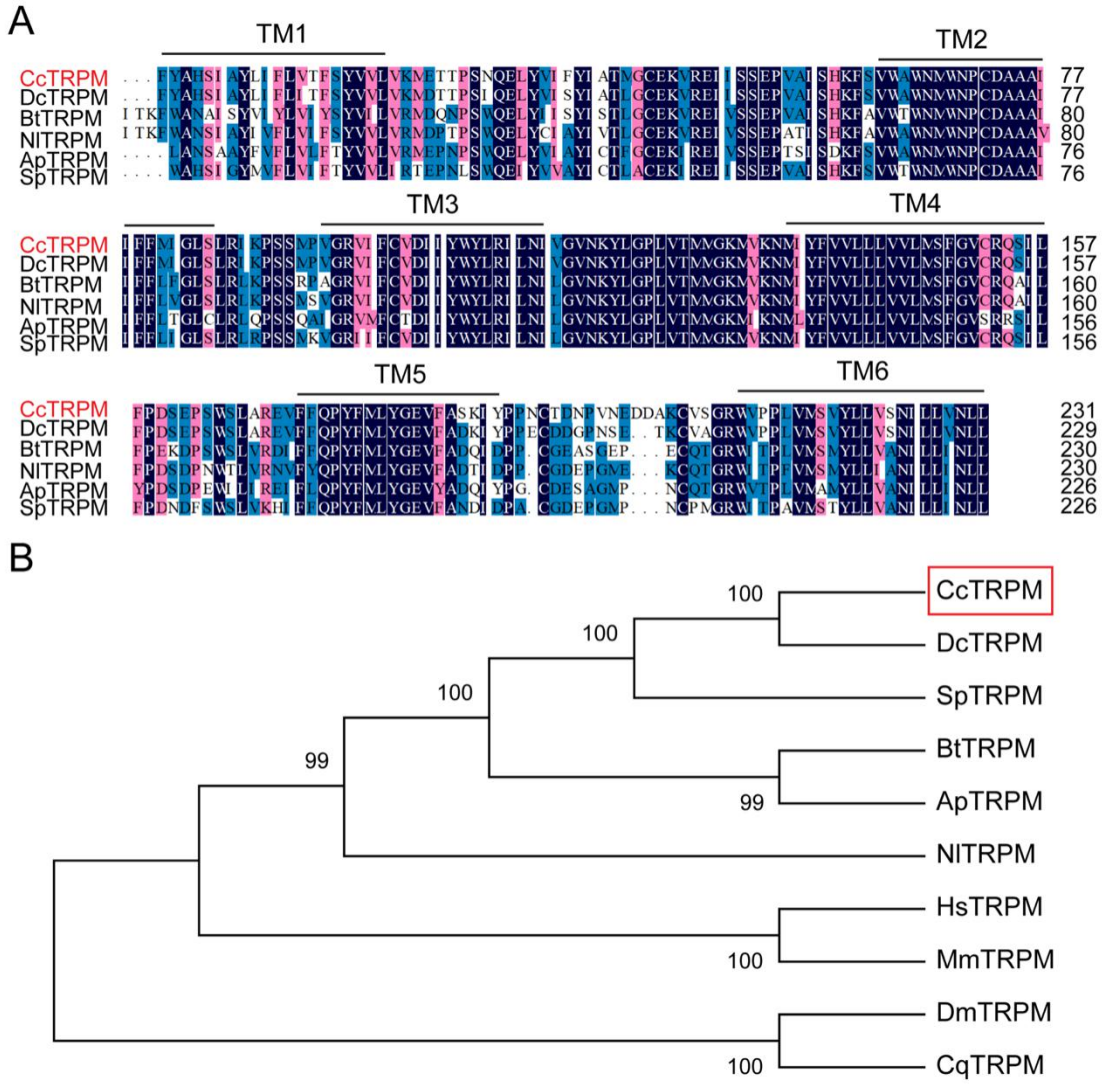

Figure S1. Sequence characterization of TRPM from different insect species.

A: Multiple alignments of the amino acid sequences of *CcTRPM* transmembrane domain with homologs from other insect species. Black represents 100% identity, red represents 75% identity and blue represents <75% identity. The transmembrane domain of TM1 to TM6 are indicated by black horizontal line. *CcTRPM* (*C. chinensis*, OQ658558), *DcTRPM* (*Diaphorina citri*, XP_017299512.2), *BtTRPM* (*Bemisia tabaci*, XP_018904971.1), *NlTRPM* (*Nilaparvata lugens*, AOR81476.1), *ApTRPM* (*Acyrthosiphon pisum*, XP_003245193.1), *SpTRPM* (*Schistocerca piceifrons*, XP_047116036.1). The same as below.

B: Phylogenetic tree analysis of *CcTRPM* and its homologs in other nine insect species. *HsTRPM* (*Homo sapiens*, NP_001384540.1), *MmTRPM* (*Mus musculus*, AAL79553.1), *DmTRPM* (*Drosophila melanogaster*, NP_001401007.1), *CqTRPM* (*Culex quinquefasciatus*, XP_038115236.1).

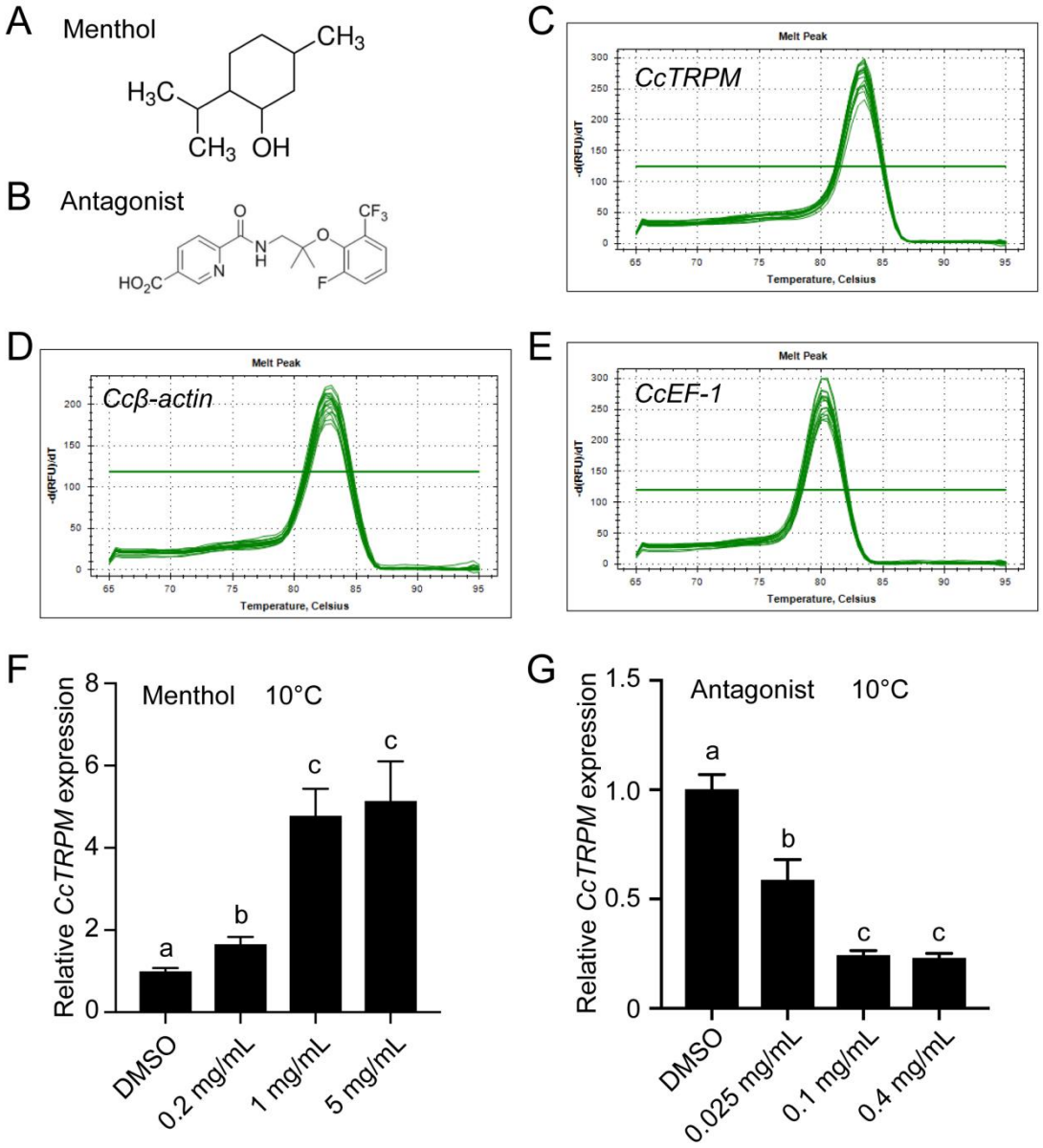

Figure S2. Effect of menthol and *CcTRPM* antagonist treatment on the mRNA expression of *CcTRPM* under 10 °C condition.

A-B: The chemical structure of menthol and TRPM antagonist.

C-E: Melting curve for qRT-PCR primers of *CcTRPM*, *Ccβ-actin* and *CcEF-1*.

F: Effect of menthol treatment at different concentrations on the mRNA expression of *CcTRPM* under 10 °C condition.

G: Effect of TRPM antagonist treatment at different concentrations on the mRNA expression of *CcTRPM* under 10 °C condition.

Data are shown as mean ± SD with three biological replications. Different letters above the bars indicated statistically significant differences ($p < 0.05$), as determined by ANOVA followed with a Turkey's HSD multiple comparison test in SPSS 20.0 software.

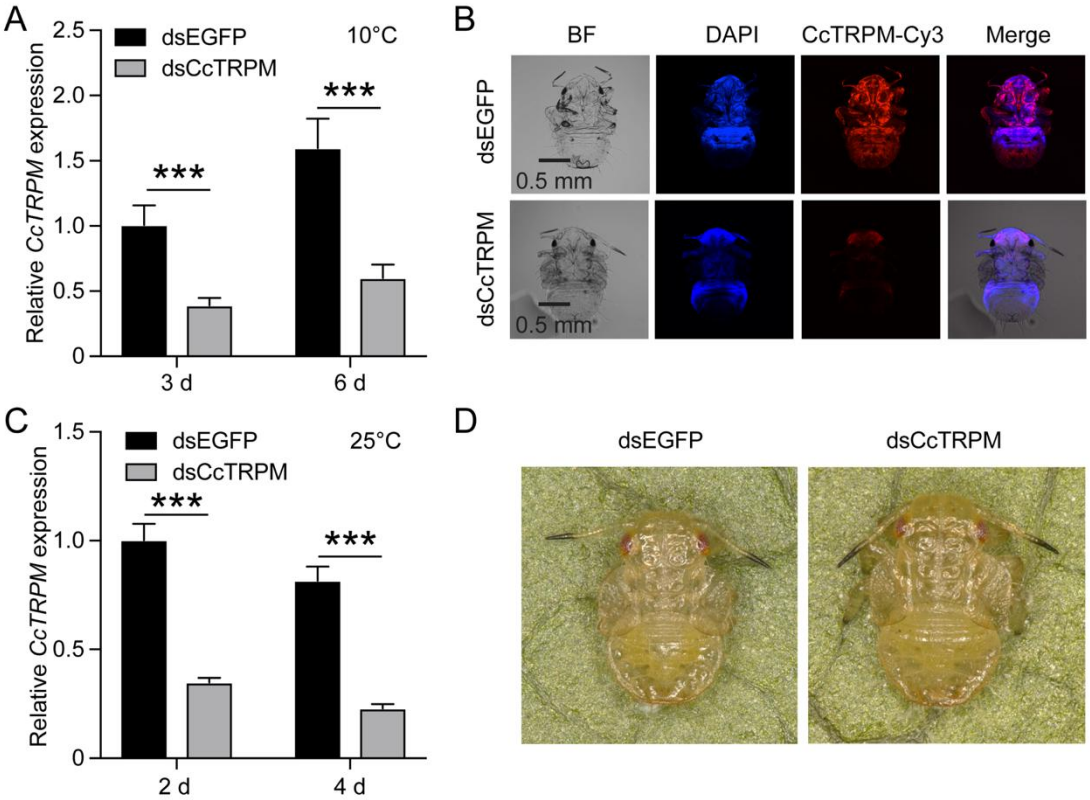

Figure S3. RNAi efficiency of *CcTRPM* and effect of *CcTRPM* knockdown on the phenotype at 25 °C.

A: RNAi efficiency of *CcTRPM* after dsCcTRPM treatment at 3 d and 6 d by qRT-PCR under 10 °C condition.

B: Representative confocal images of *CcTRPM* after SF 1st instar nymphs treated with dsCcTRPM for 6 d at 10 °C by FISH. Scale bar is 0.5 mm. BF: the bright field. DAPI: the cell nuclei were stained with DAPI and visualized in blue. CcTRPM-Cy3: CcTRPM signal was labeled with Cy3 and visualized in red. Merge: merged imaging of BF, DAPI, and CcTRPM-Cy3 signals.

C: RNAi efficiency of *CcTRPM* after dsCcTRPM treatment at 2 d and 4 d by qRT-PCR under 25 °C condition.

D: The phenotype of SF 1st instar nymphs treated with dsEGFP and dsCcTRPM at 10 d under 25 °C condition.

Data are shown as mean ± SD with three biological replications. Statistically significant differences were determined with the pair-wise Student's *t*-test, and significance levels were denoted by *** ($p < 0.001$).

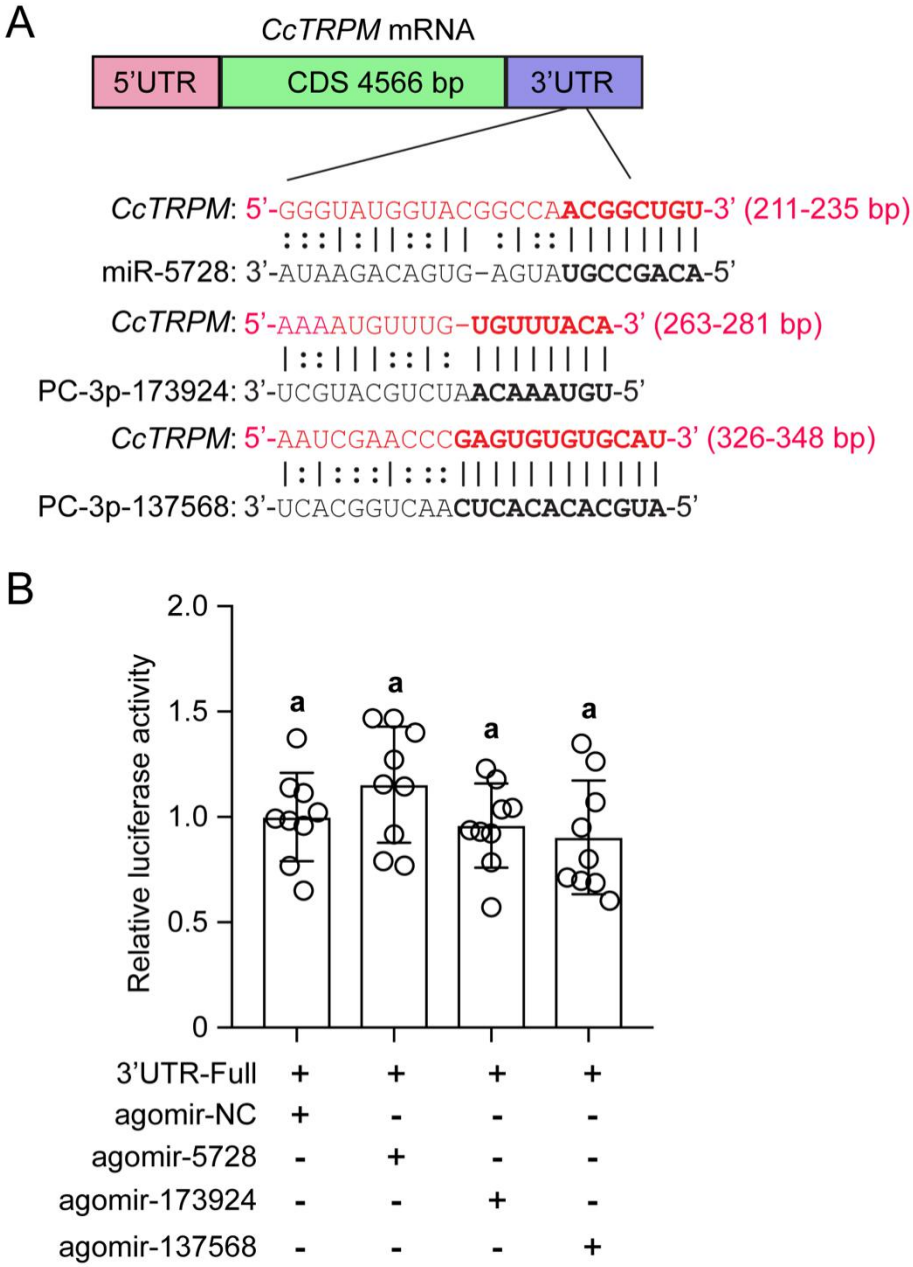

Figure S4. Validation of the target interactions between *CcTRPM* and other three miRNAs. A: The putative binding sites of miR-5728, PC-3p-173924, and PC-3p-137568 in *CcTRPM* 3'UTR were predicted by miRanda and Targetscan.

B: In vitro validation of the target interactions between miR-5728, PC-3p-173924, and PC-3p-137568 with *CcTRPM* by dual luciferase reporter assays. Data are presented as mean ± SD with nine biological replications. Different letters above the bars indicated statistically significant differences ($p < 0.05$), as determined by ANOVA followed with a Turkey's HSD multiple comparison test in SPSS 20.0 software.

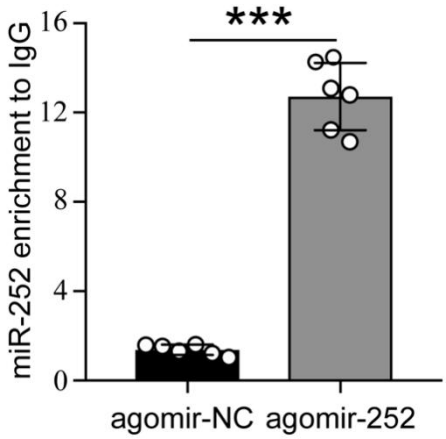

Figure S5. Transcript of miR-252 was significantly enriched by antibody against Ago1 in agomir-252 treated group compared with agomir-NC group.

Data are shown as mean ± SD with two biological replications of three technical replicates for each biological replication. Statistically significant differences were determined with the pair-wise Student's *t*-test, and significance levels were denoted by *** ($p < 0.001$).

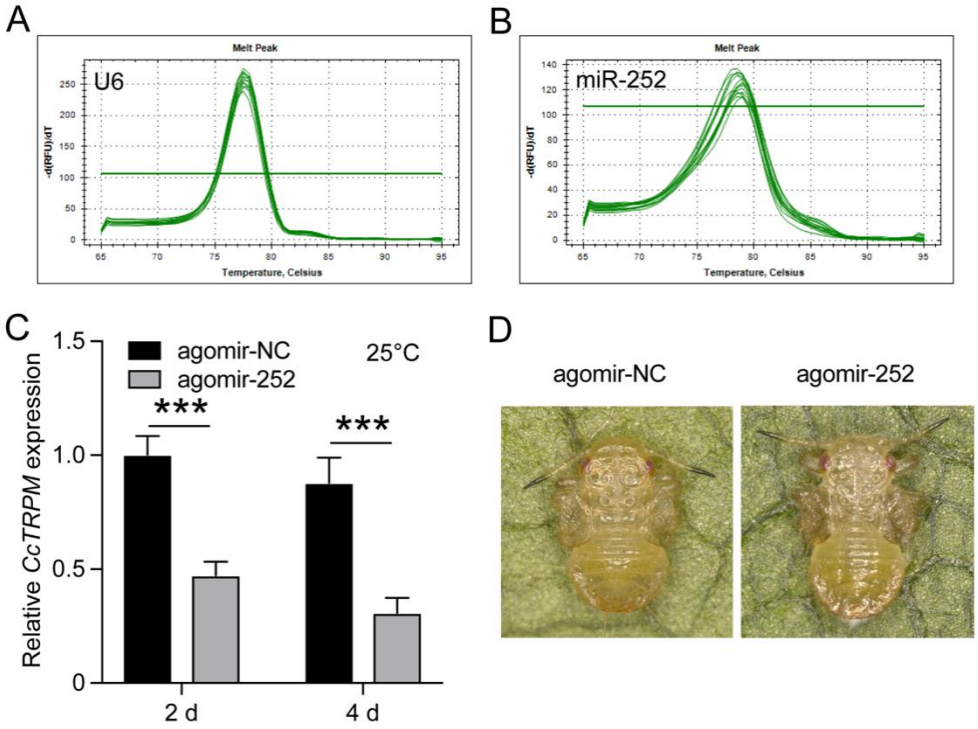

Figure S6. Effect of agomir-252 on the phenotype of SF 1st instar nymphs at 25 °C.

A-B: Melting curve for qRT-PCR primers of U6 and miR-252.

C: Effect of agomir-252 treatment 2 d and 4 d on the mRNA expression of *CcTRPM* under 25 °C condition.

D: The phenotype of SF 1st instar nymphs treated with agomir-NC and agomir-252 at 10 d at 25 °C.

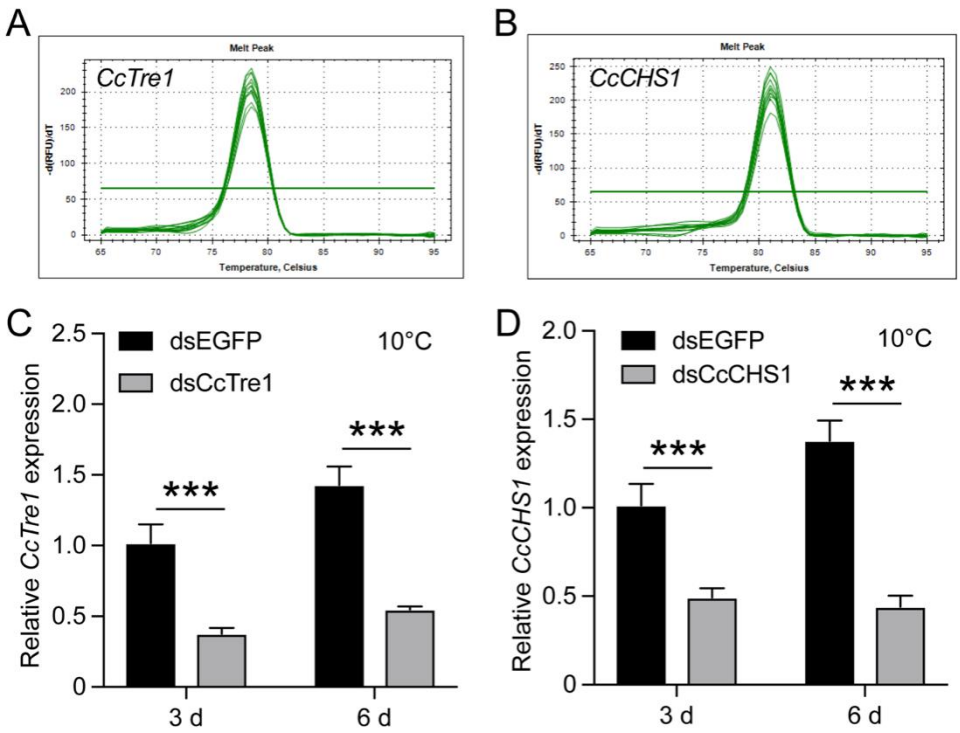

Figure S7. RNAi efficiency of *CcTre1* and *CcCHS1* at 10 °C by qRT-PCR.

A-B: Melting curve for qRT-PCR primers of *CcTre1* and *CcCHS1*.

C-D: RNAi efficiency of *CcTre1* and *CcCHS1* after dsCcTre1 and dsCcCHS1 treatment at 3 d and 6 d under 10 °C condition by qRT-PCR, respectively.

Data are shown as mean ± SD with three biological replications. Statistically significant differences were determined with the pair-wise Student's *t*-test, and significance levels were denoted by *** ($p < 0.001$).

1082 **Table S1. The primers used in current study.**

1083

Gene name (Abbreviation)	Accession number	Sequences (5'-3')	Production length (bp)	Purpose	Amplification efficiency
CcTRPM	OQ658558	Full-F1: GGATAGAGGCAACTTTTCAA Full-R1: ATCTATTCTGTCGTGCTCCA	1307	RT-PCR for sequence validation	—
		Full-F2: TAGACGAAGCCATGATGC Full-R2: ACAACTGTTTCACGGAGTGT	1162	RT-PCR for sequence validation	—
		Full-F3: TAGCCAGACATTCTCAACAA Full-R3: GAAGCATTACTATGGGTTGC	1436	RT-PCR for sequence validation	—
		Full-F4: AGCAGACCCTTTCCACTC Full-R4: TAACTGTTAACACATTGTTTCTGC	1334	RT-PCR for sequence validation	—
		qF: ACAATGCATTCTTCTTGACC qR: GACTTTGTACACTGGGGGTA	141	qRT-PCR	102.57
		RNAi-F1: GATCACTAATACGACTCACTATAGGGAGA GGTACCTTCGTATCCTCAAC RNAi-R1: GATCACTAATACGACTCACTATAGGGAGA TGGCATTGATCTCCATGAAA	472	dsRNA synthesis	—

		Probe: Cy3-CATAGATCGCGTAGGAGGTC	20	FISH	—
		3’UTR-Full-F1: CTAGTTGTTTAAACGAGCTC CATTATGTAACCACAGCGTAA 3’UTR-Full-R1: TGCATGCCTGCAGGTCGACTCTAGA TTCCTAGAAACTCAAAAATCG	419	Amplification of 3’UTR full sequence	—
		3’UTR-Mut-F1: CTAGTTGTTTAAACGAGCTC CATTATGTAACCACAGCGTAA 3’UTR-Mut-R1: TGCATGCCTGCAGGTCGACTCTAGA AAGTACTATCCACGCTCGAC	137	Amplification of 3’UTR mutant sequence	—
		Orf-F: GGACGAGCTGTACAAGTAGGGATCC ATGGAGAGGTCCCAGAGGTC Orf-R: GTTTAAACGGGCCCTCTAGACTCGAGC TTAACACATTGTTTCTGCGC	4618	Amplification of orf sequence	—
miR-252	-	qF: GCTAAGTACTGGTGCCGCAGGA	—	qRT-PCR	—
U6	-	qF: AGGATGACACGCAAAATCGT	—	qRT-PCR	—
CcTre1	OQ734934	qF: GGAACTCCCTCCTCTATGTT qR: CCAATAGTCAGCCAATCTGT	147	qRT-PCR	97.73

		RNAi-F1: GATCACTAATACGACTCACTATAGGGAGA AGATGTCAAAACCAATCCAG RNAi-R1: GATCACTAATACGACTCACTATAGGGAGA GGCCAAGTTGTAGTATTTGC	455	dsRNA synthesis	—
CcTre2	OQ734935	qF: CCAATCCTTCTCTACACCTG qR: CTGTCATTGTTGTACGGTTG	123	qRT-PCR	93.68
CcTre-like	OQ734936	qF: GACCGAACCTATGATCTCAA qR: AGATGTACCAAGCTGCTGAG	135	qRT-PCR	106.13
CcCHS1	OQ658570	F: AGAAGAGAAGAAACAGCAGG R: TAGTGTCCAATCGTTTCTCC	233	qRT-PCR	101.47
		RNAi-F1: GATCACTAATACGACTCACTATAGGGAGA TTGGCTACCACTGAGAAACT RNAi-R1: GATCACTAATACGACTCACTATAGGGAGA ATGCGTTTCGTACTCGTAAT	367	dsRNA synthesis	—
CcCHS2	OQ658569	F: TATTAGGCTGATGTTGCTGA R: GAGGCAACACAAGAGGTAAG	124	qRT-PCR	95.49
CcHK1	OQ658562	F: GAGTCTGCCATCTACTGTCC	130	qRT-PCR	96.21

		R: CGGGGGTGATATTTGTATAG			
CcHK2	OQ658560	F: AAATAGTCCGACTGGCATTA R: TGTACTCTTGGGCTCACTTT	137	qRT-PCR	98.05
CcHK3	OQ658561	F: AGCATTTGAGAGAGAACGTG R: CCGCTGATATTGTCTTCTTC	120	qRT-PCR	103.51
CcG6PI	OQ658563	F: CCTGCTATCTCTCACAATCC R: CTTTCAGTTCAGCTTCTGCT	127	qRT-PCR	107.23
CcGFAT	OQ658564	F: ACTGAAACATGGACCTCTTG R: CTTCCATCTCTGGCAATAAC	123	qRT-PCR	97.06
CcGNA	OQ658565	F: GGCGAGTATTTTGTGAGTGT R: CTCGGTACGTATCATCGACT	145	qRT-PCR	108.46
CcAGM	OQ658566	F: TTTATTTTGAGGCAAATGGT R: AAGAGTCTCCGACAGTTTCA	138	qRT-PCR	102.84
CcUAP1	OQ658567	F: TGGGGAACTTGTGTATAACC R: TGGAATCTTCTTGAGTGCTT	124	qRT-PCR	98.03
CcUAP2	OQ658568	F: ACATTGACTCCAAAGGATTG R: GGCAAAATCATGTTCTCTGT	134	qRT-PCR	89.74

CcEF-1	OQ658572	qF: TGTGTCGAGTCATTCTCTGA qR: TTACTTTACCGGAGGACAGA	124	Reference gene for qRT-PCR	98.63
Ccβ-Actin	OQ658571	qF: CAGCACCATGAAGATCAAG qR: GACTCGTCATACTCCTGCTT	129	Reference gene for qRT-PCR	102.87
EGFP	ACY56286	F: GATCACTAATACGACTCACTATAGGGAGA CTCCAGCAGGACCATGTGATC R: GATCACTAATACGACTCACTATAGGGAGA CCTGAAGTTCATCTGCACCAC	596	dsRNA synthesis	—

1084

1085 Note: The black boxes indicated the T7 promoter sequences in the primers of dsRNA synthesis. The underlines showed the homologous arm sequences for the

1086 seamless cloning in homologous recombination.

1087